Banner appropriate to article type will appear here in typeset article

Poromechanical modelling of responsive hydrogel pumps

Joseph J. Webber† and Thomas D. Montenegro-Johnson

Mathematics Institute, University of Warwick, Coventry CV4 7AL, UK

Thermo-responsive hydrogels are smart materials that rapidly switch between hydrophilic (swollen) and hydrophobic (shrunken) states when heated past a threshold temperature, resulting in order-of-magnitude changes in gel volume. Modelling the dynamics of this switch is notoriously difficult, and typically involves fitting a large number of microscopic material parameters to experimental data. In this paper, we present and validate an intuitive, macroscopic description of responsive gel dynamics and use it to explore the shrinking, swelling and pumping of responsive hydrogel displacement pumps for microfluidic devices. We finish with a discussion on how such tubular structures may be used to speed up the response times of larger hydrogel smart actuators and unlock new possibilities for dynamic shape change.

1. Introduction

Hydrogels are soft porous materials comprising a cross-linked, hydrophilic, polymer structure surrounded by adsorbed water molecules that are free to move through the porous scaffold (Doi 2009; Bertrand *et al.* 2016). Though simple in structure, their elastic and soft nature, coupled with the ability to change volume to an extreme degree by swelling or drying, affords them a number of uses in engineering, medical sciences and agriculture (Zohuriaan-Mehr *et al.* 2010; Guilherme *et al.* 2015). In traditional hydrogels, this swelling and drying occurs passively. In responsive hydrogels, the affinity of the polymer scaffold for water changes as a result of external stimuli such as heat, light or chemical concentration (Neumann *et al.* 2023), allowing for controllable swelling-shrinking cycles. Such 'smart' materials with tunable shape-changing behaviour have applications in soft robotics (Lee *et al.* 2020), microfluidics (Dong & Jiang 2007), and in models of biological processes (Vernerey & Shen 2017).

Though responsive gels can react to stimuli of various forms, the most ubiquitous are thermo-responsive gels, where the affinity of the polymer chains for water drops rapidly at

† Email address for correspondence: joe.webber@warwick.ac.uk

Abstract must not spill onto p.2

a critical temperature T_C. Above this lower critical solution temperature (LCST), hydrogen bonds holding the water molecules in place around the polymer chains break and the release of water molecules is entropically favoured. Perhaps the most widely-studied thermo-responsive gel is poly(N-isopropylacrylamide) (PNIPAM), which has an LCST that can be tuned to be close to room temperature, and finds a number of medical applications owing to its biocompatibility (Das *et al.* 2015). The effect of deswelling is significant, with many such gels exhibiting an order-of-magnitude volume change at T_C, opening up the possibility of a number of macroscopic use cases for responsive gels (Voudouris *et al.* 2013).

Modelling the dynamics of this shape change is difficult, and is thus often restricted to simpler geometries such as spheres (Tomari & Doi 1995). The typical modelling approach seeks the dependence of the Helmholtz free energy of the gel on the ambient temperature, encoded by the Flory χ parameter, representing the attraction between water molecules and polymer chains. This parameter typically decreases with increasing temperature (Cai & Suo 2011), but its value is usually deduced from fitting to experimental data (Afroze *et al.* 2000). Accurately determining the χ parameter is a long-standing problem in polymer physics, with experimental approaches often difficult, owing to the number of different physical processes underpinning solvent–polymer and polymer–polymer interactions, with some more recent work using machine learning approaches (Nistane *et al.* 2022) to seek patterns in the variation of χ with polymer structure. Difficulties are further compounded by the fact that small changes in χ can lead to large differences in the physics of hydrogels (Afroze *et al.* 2000).

The Helmholtz free energy is then minimised with respect to deformation, determining the equilibrium swelling state at a fixed temperature. However, describing the transient evolution of the state of the hydrogel as the temperature is varied is significantly more difficult, and requires the separate consideration of chemical potentials, polymer network elasticity and induced interstitial flows through the gel.

In classic large-strain poroelastic models (Bertrand *et al.* 2016), the principal stresses (in the directions of the principal stretches) are deduced from the energy. These stresses are then balanced with gradients in chemical potential to describe the poroelastic flow, and thus the gel dynamics. Whilst effective, these models rely on a characterisation of the material in terms of a large number of microscopic parameters, are computationally expensive, and result in a series of coupled partial differential equations for porosity, chemical potential and stresses, which potentially masks some of the key macro-scale physics driving the responsive dynamics and offers limited potential for analytical solutions.

It is also possible to model the behaviour of deformable soft porous media using the theory of linear poroelasticity, characterising the gel by its elastic moduli and describing the flow through the scaffold using Darcy's law (Doi 2009). These models are inherently macroscopic, and offer the benefit of analytic tractability. However, they cannot cope with nonlinearities that arise from large swelling strains, and are therefore unsuitable for modelling super-absorbent gels, where the volumetric changes involved in swelling and drying may be of the order of 10 to 100 times (Bertrand *et al.* 2016).

In this work, we therefore seek a model based only on macroscopically-measurable material properties that can also incorporate large swelling strains and give faster predictions to describe the transient swelling–deswelling states in response to temperature changes. Such a model would be valuable, as it could provide rapid quantitative design input to experimentalists working on applications of responsive gels such as small microfluidic devices (Harmon *et al.* 2003) and robotic actuators (Lee *et al.* 2020).

A macroscopic continuum-mechanical model for passive gels was recently provided by Webber & Worster (2023) and Webber *et al.* (2023). The model allows for nonlinearities in the isotropic strain, whilst linearising around small deviatoric strains. This assumption is equivalent to the statement that, at any swelling state, the hydrogel material acts as a linear-

(a) Reference state   (b) Stress decomposition
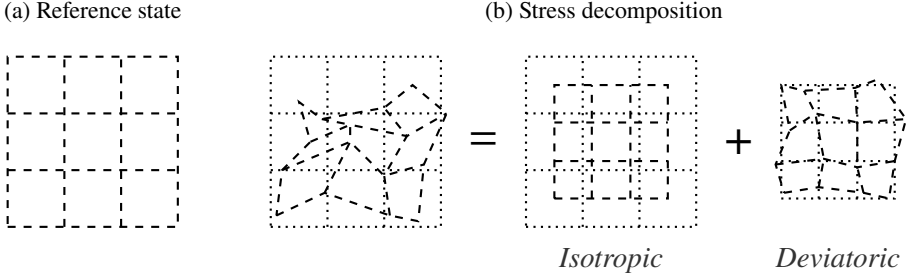
Isotropic   *Deviatoric*

Figure 1: On the left, the reference state where $\phi \equiv \phi_0$ and the cross-linked polymers are in thermodynamic equilibrium with the surroundings. On the right, a schematic decomposition of any deformation (dashed lines) from this reference state (dotted lines) into an isotropic part due to drying (in this case) and a small deviatoric part.

elastic bulk solid, and it reduces the gel dynamics to a nonlinear advection-diffusion equation for the local polymer (volume) fraction ϕ. In this paper, we extend this model to incorporate thermo-responsive effects, by assuming that the osmotic pressure (and potentially other material parameters) can depend also on temperature. This dependency leads to different swelling behaviour as the temperature is varied, and different equilibrium states either side of the LCST.

Our model makes the analysis of complicated responsive actuators more tractable, and provides good qualitative and quantitative predictions of the key physics at play. It is broadly applicable to a range of hydrogel actuators in microfluidic devices, such as valves (Dong & Jiang 2007), passive pumps (drawing in water through their swelling behaviour) (Seo *et al.* 2019), and the displacement pumps (Richter *et al.* 2009) that we will consider herein.

In this paper, we analyse the contraction of a hollow tube formed of thermo-responsive hydrogel when a heat pulse is applied, and, using the thermo-responsive linear-elastic-nonlinear-swelling model derived in section 2, we deduce both the shrunken geometry and the transition from swollen to shrunken states by the flow of water through the hydrogel walls and the hollow lumen of the 'pipe'.

Notably, we show that the presence of a fluid-filled pore in the centre of a tube enables much faster responses to changes in temperature than in a pure gel, since the flow that results from deswelling is not restricted by viscous resistance through the pore matrix. Our model also gives expressions for the pumping rate and characteristics of the induced peristaltic fluid flow in response to propagating heat pulses.

Finally, we note that in addition to applications driving fluid flow in microfluidic devices, a number of existing applications depend on the ability to tune response times to external stimuli (Maslen *et al.* 2023). In such constructions, anisotropic shape changes result from isotropic deswelling that occurs at different rates – so-called "dynamic anisotropy" – in response to a heat pulse. This behaviour is key to unlocking non-reciprocal shrinking-swelling dynamics, critical for achieving work in the inertialess fluid regime. The existence of a simplified, analytic, understanding of thermo-responsive gels allows us to tune the thickness of the pipe walls to give a desirable response time, affording us predictions for the construction of responsive hydrogel devices with controllable response rates to external stimuli, irrespective of the intrinsic material response rate. We begin with the derivation of the governing equations that would underpin the responses of such devices.

2. Thermo-responsive linear-elastic-nonlinear-swelling model

The linear-elastic-nonlinear-swelling (LENS) model introduced in Webber & Worster (2023) and Webber *et al.* (2023) is a poromechanical continuum model for the behaviour of large-swelling gels. The model is derived based upon the assumption that isotropic strains, corresponding to the swelling and drying of a gel, may be large, but deviatoric strains must be small. This model achieves both the accurate description of large deformation seen in nonlinear energy-based models and the analytic tractability of linear poroelasticity. Figure 1 shows how a general deformation from a reference state can be decomposed into these two parts, and illustrates how we can view isotropic shrinkage or growth as drying or swelling, respectively, changing the local polymer volume fraction ϕ. In this model, at any given degree of swelling, a hydrogel is characterised using three swelling-dependent material parameters; a generalised osmotic pressure $\Pi(\phi)$ representing the gel's affinity for water, a shear modulus $\mu_s(\phi)$ representing the resistance to elastic deformation and a permeability $k(\phi)$ representing the ease with which water can percolate through the gel scaffold.

In addition to the comparative simplicity of such an approach, these three parameters correspond to clear physical processes, as opposed to microscopic forces on the scale of the polymer chains, or thermodynamic constants that can be difficult to relate to larger-scale swelling or drying phenomena. For example, when applying a force to a gel, the initial, incompressible, response is mediated by the shear modulus μ_s, the final steady state as water is driven in or imbibed is set by the generalised osmotic pressure Π, and the timescale over which this occurs is set by the permeability k. These parameters can be determined for any hydrogel without an understanding of the micro-scale structure or the thermal physics governing the osmotic and elastic behaviour of these materials.

This is of particular use when considering thermo-responsive gels, where a large number of parameters such as the cross-linker density and interaction parameters must be estimated from reference values or curve fitting (Hirotsu *et al.* 1987). Perhaps the clearest illustration of the distinction between our macroscopic model and models based on micro-scale physics is our generalised osmotic pressure Π. This differs from the osmotic pressures in the hydrogel literature by also incorporating isotropic elastic stresses on gel elements, as well as the affinity of polymer chains for water (Webber 2024). Phenomenologically, the two effects are indistinguishable, and lead to expulsion or imbibition of water, even though their physical basis is vastly different (Peppin *et al.* 2005), and we will henceforth refer to our parameter Π simply as the *osmotic pressure* for this reason.

Thermo-responsive hydrogels respond to changes in temperature through rapidly losing their affinity for water when the lower critical solution temperature (LCST) is exceeded. Macroscopically, this manifests itself as the expulsion of water from the pore spaces and the drying out of the remaining polymer scaffold as a result. This corresponds to a raising of the equilibrium polymer fraction (the polymer fraction attained by a gel placed in water with no external constraints) ϕ_0 as a result of the change in temperature, and we incorporate this effect into a LENS model by introducing a temperature-dependent equilibrium polymer fraction $\phi_0(T)$. By definition, the osmotic pressure is zero when $\phi = \phi_0$, and so in order to accommodate thermo-responsivity into our model, we must allow the osmotic pressure to depend on T, with

$$\Pi = \Pi(\phi, T) \quad \text{and} \quad \Pi(\phi_0(T), T) = 0. \tag{2.1}$$

In figure 2 we illustrate two potential forms of the osmotic pressure below and above the critical temperature T_C, and show the mechanism for transition between the equilibrium swelling states $\phi_0(T_1)$ and $\phi_0(T_2)$ as the temperature is raised and a hydrogel deswells.

In experiments, it is observed that the equilibrium polymer fraction rises rapidly as the threshold $T = T_C$ is crossed, with little variation in $\phi_0(T)$ either side of this critical
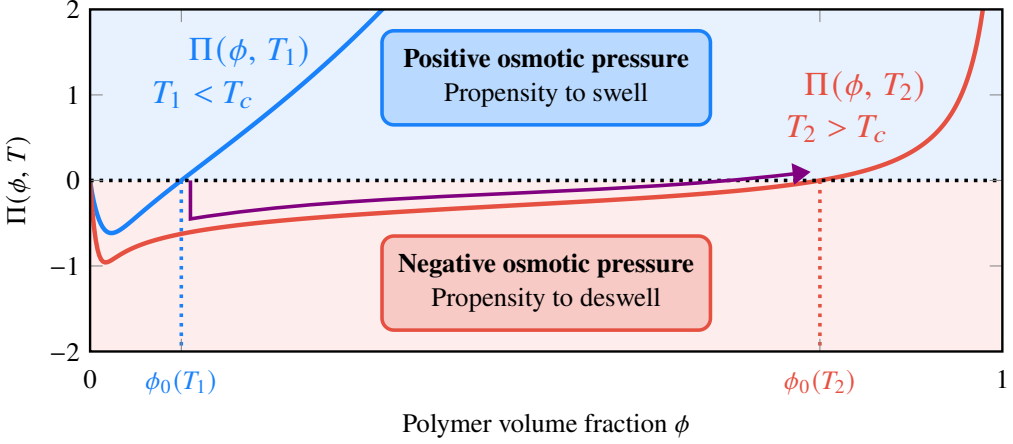
Figure 2: Plots of a representative osmotic pressure function at a temperature T_1 below the lower critical solution temperature T_C and T_2 above this threshold, showing how the equilibrium polymer fraction increases sharply as the temperature is raised. A sample trajectory as the temperature is raised from T_1 to T_2 is plotted.

temperature (Butler & Montenegro-Johnson 2022). This motivates the choice of a piecewise constant equilibrium polymer fraction

$$\phi_0(T) = \begin{cases} \phi_{00} & T \leqslant T_C \\ \phi_{0\infty} & T > T_C \end{cases}, \tag{2.2}$$

where $\phi_{0\infty}$, the 'deswollen' equilibrium polymer fraction, is greater than that in the 'swollen' state, ϕ_{00}. The simplest continuous osmotic pressure functions that capture positivity above the equilibrium and negativity below it are defined by

$$\Pi(\phi, T) = \begin{cases} \Pi_{00} \dfrac{\phi - \phi_{00}}{\phi_{00}} & T \leqslant T_C \\ \Pi_{0\infty} \dfrac{\phi - \phi_{0\infty}}{\phi_{0\infty}} & T > T_C \end{cases}, \tag{2.3}$$

akin to the linearised osmotic pressures used in Webber & Worster (2023), with the parameters Π_{00} and $\Pi_{0\infty}$ representing the strength of the osmotic pressures when the polymer fraction is perturbed from its equilibrium value. In the present study, we use the expressions of equations (2.2) and (2.3) for their analytic simplicity and their ability to capture the macroscopic deswelling behaviour as the LCST is crossed, but in principle any expression for the osmotic pressure can be substituted into the LENS model. Indeed, in appendix A, we illustrate how LENS parameters can be deduced from a standard model for thermo-responsive gels, employing a neo-Hookean elastic model for the polymer chains and Flory-Huggins theory for the mixing of water and polymer molecules (Cai & Suo 2011).

To model the stresses and strains on a hydrogel element, we measure the displacement $\boldsymbol{\xi}$ from a fixed reference state. In Webber & Worster (2023), this was chosen to be the "fully swollen" equilibrium state $\phi \equiv \phi_0$, but we must pick a temperature-independent reference when gels are thermo-responsive. We choose some reference temperature $T_0 < T_C$ where $\phi_0 = \phi_{00}$ and consider this the fully-swollen reference state relative to which all displacements

are measured. Therefore, the Cauchy strain is equal to

$$\boldsymbol{e} = \left[1 - \left(\frac{\phi}{\phi_{00}} \right)^{1/3} \right] \boldsymbol{I} + \epsilon, \tag{2.4}$$

with ϵ the traceless deviatoric strain, assumed small in LENS modelling. This shows that the divergence of the displacement field satisfies

$$\boldsymbol{\nabla} \cdot \boldsymbol{\xi} = 3 \left[1 - \left(\frac{\phi}{\phi_{00}} \right)^{1/3} \right]. \tag{2.5}$$

The stresses on an element of gel are given by the Cauchy stress tensor

$$\sigma = - \left[p + \Pi(\phi, T) \right] \boldsymbol{I} + 2\mu_s(\phi)\epsilon, \tag{2.6}$$

where p is the pervadic, or Darcy, pressure (the fluid pressure as would be measured by a transducer separated from the gel by a partially-permeable membrane that only allows water to pass, Peppin *et al.* (2005)). Gradients in pervadic pressure p drive interstitial fluid flows relative to the polymer scaffold, giving a net volume flux $\boldsymbol{u}$ of water via Darcy's law,

$$\boldsymbol{u} = -\frac{k(\phi)}{\mu_l} \boldsymbol{\nabla} p, \tag{2.7}$$

where $k(\phi)$ is the polymer fraction-dependent permeability, which we assume to be equal to a constant k for simplicity. Note that this Darcy velocity is not equal to the water velocity $\boldsymbol{u_w}$ – instead, it is equal to the flux of water relative to a polymer scaffold that deforms with velocity $\boldsymbol{u_p}$, so $\boldsymbol{u} = (1 - \phi)(\boldsymbol{u_w} - \boldsymbol{u_p})$. An expression for the polymer velocity $\boldsymbol{u_p}$ is derived in Webber *et al.* (2023),

$$\boldsymbol{u_p} = \left(\frac{\phi}{\phi_{00}} \right)^{-1/3} \frac{\partial \boldsymbol{\xi}}{\partial t}, \tag{2.8}$$

representing the reconfiguration of the polymer scaffold as a gel deforms in terms of the displacement field. It can also be shown that the phase-averaged flux $\boldsymbol{q} = \phi \boldsymbol{u_p} + (1 - \phi)\boldsymbol{u_w} = \boldsymbol{u} + \boldsymbol{u_p}$ is solenoidal, through conservation of water and polymer.

As shown in the stress tensor of equation (2.6), deviatoric elastic strains are related to stresses via the shear modulus $\mu_s(\phi)$, which we henceforth take as a constant μ_s, independent of polymer fraction. This both leads to a more analytically-tractable model, but is also predicted by fully-nonlinear energy-based models, such as those based on neo-Hookean polymer chain elasticity, as outlined in appendix A.

Combining the separate expressions for polymer and water conservation with Cauchy's momentum equation, gel dynamics are governed by the polymer fraction evolution equation

$$\frac{\partial \phi}{\partial t} + \boldsymbol{q} \cdot \boldsymbol{\nabla} \phi = \boldsymbol{\nabla} \cdot [D(\phi)\boldsymbol{\nabla}\phi] \quad \text{with} \quad D(\phi) = \frac{k}{\mu_l} \left[\phi \frac{\partial \Pi}{\partial \phi} + \frac{4\mu_s}{3} \left(\frac{\phi}{\phi_0} \right)^{1/3} \right]. \tag{2.9}$$

The same derivation, presented for example in Webber & Worster (2023) and Webber (2024), shows that the fluid flux (2.7) can be written as $[D(\phi)/\phi] \boldsymbol{\nabla}\phi$, such that water flows from areas with low ϕ towards drier regions with high ϕ. Equation (2.9) can then be coupled with boundary conditions on this flow field and on the stress (2.6) to solve for the evolution of composition in time. Techniques outlined in Webber *et al.* (2023) allow for the shape of the gel to be deduced from its composition, solving a biharmonic equation for the displacement field $\boldsymbol{\xi}$, but for the simple geometries considered in this paper, equation (2.5) alongside symmetry assumptions will suffice.

223 ## 2.1. *Comparing thermo-responsive LENS with a fully-nonlinear model*

224 To show that the predictions of LENS modelling compare well with those of commonly-used
225 nonlinear modelling of thermo-responsive hydrogels, we consider the swelling and drying of
226 a poly(N-isopropylacrylamide) (PNIPAM) sphere when heated or cooled around its critical
227 temperature T_C. This problem has been treated extensively in the literature owing to its
228 geometric simplicity and tractability (Matsuo & Tanaka 1988; Tomari & Doi 1995; Butler &
229 Montenegro-Johnson 2022). Since no constitutive laws for material parameters are specified
230 in LENS, we can deduce functional forms for $\Pi(\phi)$, $\mu_s(\phi)$ and $k(\phi)$ given any model of our
231 choice, including the fully-nonlinear models used by other authors.

232 Starting from the most common approach of choosing a Gaussian-chain nonlinear elastic
233 model for the polymer scaffold coupled with Flory-Huggins theory for interaction between
234 polymer and water molecules (Cai & Suo 2011), we derive the form of $\Pi(\phi)$ in appendix A,

235 $$\Pi(\phi) = \frac{k_B T}{\Omega_f} \left[\Omega^{-1} \left(\phi - \phi^{1/3} \right) - \phi - \ln\left(1 - \phi\right) - \phi^2 \chi + \phi^2 (1 - \phi) \frac{\partial \chi}{\partial \phi} \right], \qquad (2.10)$$

236 where k_B is the Boltzmann constant, Ω_f is the volume occupied by a single water molecule,
237 Ω is the volume of polymer molecules relative to water molecules, and χ is the Flory
238 interaction parameter, quantifying the affinity of polymer chains for water molecules. This
239 osmotic pressure function permits us to deduce the equilibrium polymer fraction as a function
240 of temperature, with a sharp change at the critical temperature T_C. A similar approach gives
241 the shear modulus μ_s, that is found to be independent of polymer fraction. Then, we fit the
242 measured parameters of Hirotsu *et al.* (1987) to find the osmotic modulus, shear modulus and
243 permeability for such gels in our formalism, as detailed fully in appendix A and the electronic
244 supplementary material. This parameter set was chosen to avoid the complicated hysteresis
245 behaviour seen in other such fitting parameters (for example, those measured in Afroze *et al.*
246 (2000)), which can be modelled using our approach but we do not discuss here. A more
247 detailed discussion of differences between swelling and drying and spinodal decomposition
248 between different sets of parameters can be found in Butler & Montenegro-Johnson (2022).
249 Further details of the governing equations in both cases, and the precise forms of the non-
250 dimensional times and lengths t_{BMJ} and r_{BMJ} can be found in the supplementary material.

251 We first compute the swelling behaviour of a gel that is initially in equilibrium at $T = 308$ K
252 before the temperature is rapidly decreased to 304 K. This leads to swelling from an initial
253 polymer fraction of $\phi_0 \approx 0.64$ to a much lower value $\phi_0 \approx 0.05$. Figure 3 shows good
254 quantitative and qualitative agreement with the results of Butler & Montenegro-Johnson
255 (2022), with marginally slower growth of the radius but the same diffusive transport of water
256 from surroundings into the bulk of the gel. Repeating the same analysis for smooth drying
257 (where there is no formation of a drying front), we raise the temperature from 304 K to
258 307.6 K, with figure 4 showing the good qualitative, but weaker quantitative, agreement in
259 this case. Our model does, however, capture the rapid initial and later-time drying, with a
260 plateau of slower drying present when $2 \leqslant t_{BMJ} \leqslant 5$.

261 There is a more significant discrepancy in the predictions of LENS and the fully-nonlinear
262 model in this case due to the significant polymer fraction gradients present close to $t_{BMJ} = 5$.
263 In Butler & Montenegro-Johnson (2022), the criteria for gel deswelling with phase separation
264 are deduced, and in this smooth deswelling problem, we pass close to a region of parameter
265 space where phase separation can occur. The presence of a nearby equilibrium solution gives
266 a critical slow-down behaviour akin to that discussed by Gomez *et al.* (2017), manifesting
267 itself as the plateau of slow drying at intermediate times.

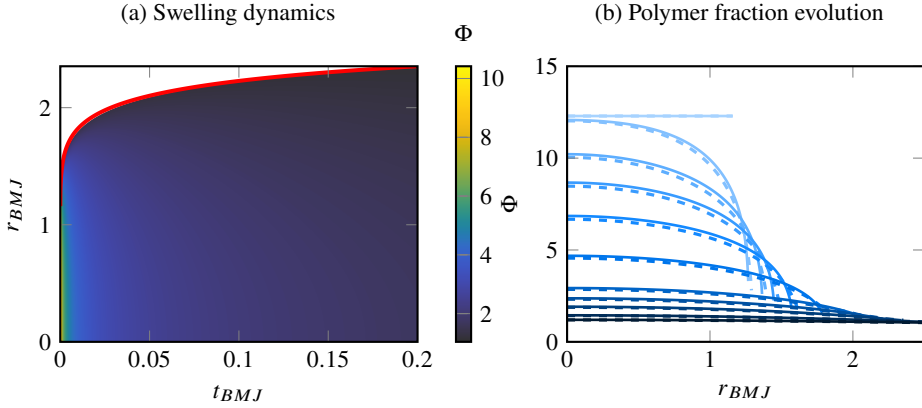(a) Swelling dynamics   (b) Polymer fraction evolution

Figure 3: Plots illustrating the swelling of a hydrogel bead after the temperature is lowered from 308 K to 304 K. The parameters used are the same as in Butler & Montenegro-Johnson (2022), with the fully nonlinear results plotted for comparison, and t_{BMJ} is the non-dimensional time used by Butler & Montenegro-Johnson. On the left, the evolving polymer fraction is shown with the growth of the radius in the fully nonlinear model shown as a red curve. On the right, porosity profiles are shown at t_{BMJ} = 0.0001, 0.0002, 0.0005, 0.001, 0.0025, 0.01, 0.05, 0.1, 0.2, 0.5 and 1, with darker blue representing later times. Results from the fully nonlinear model are shown as dashed lines.

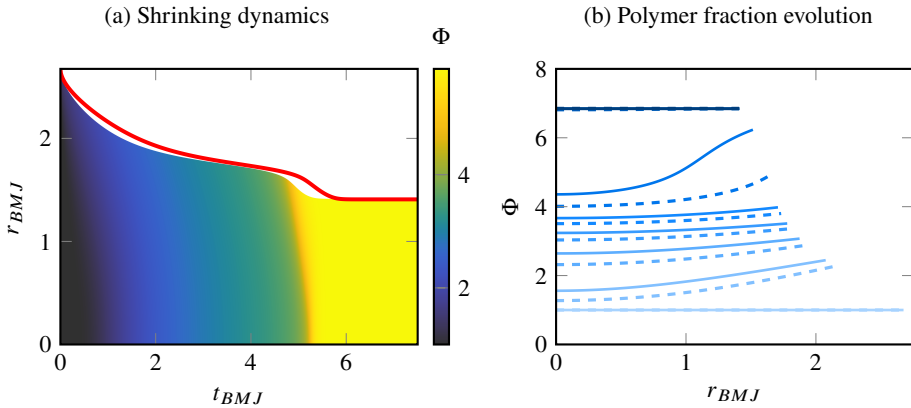(a) Shrinking dynamics   (b) Polymer fraction evolution

Figure 4: Plots illustrating the drying of a hydrogel bead after the temperature is raised from 304 K to 307.6 K, with the same parameters as before and the fully nonlinear solution plotted for comparison. On the left, the evolving porosity is shown with the shrinkage of the radius in the fully nonlinear model shown as a red curve. On the right, porosity profiles are shown at t_{BMJ} = 0, 1, 2, 3, 4, 5, 6, 7 and 8, with darker blue representing later times. Results from the fully nonlinear model are shown as dashed lines.

2.1.1. *Phase separation and negative diffusivities*

Often during the deswelling process a sharp drying front forms, travelling radially inwards through the bead, with the exterior rapidly drying to its final state and the interior remaining relatively swollen until the front reaches the centre. This occurs when trajectories in (T, ϕ)-space pass through the spinodal or coexistence regions. In the spinodal region, spontaneous phase separation can occur, with the formation of regions of dried polymer surrounded by swollen gel or vice versa as the system equilibrates. The coexistence region is a special case of this, where a dried gel and a swollen one can coexist in thermodynamic equilibrium with a simple sharp boundary (such as a drying front) separating the two. In the present study,
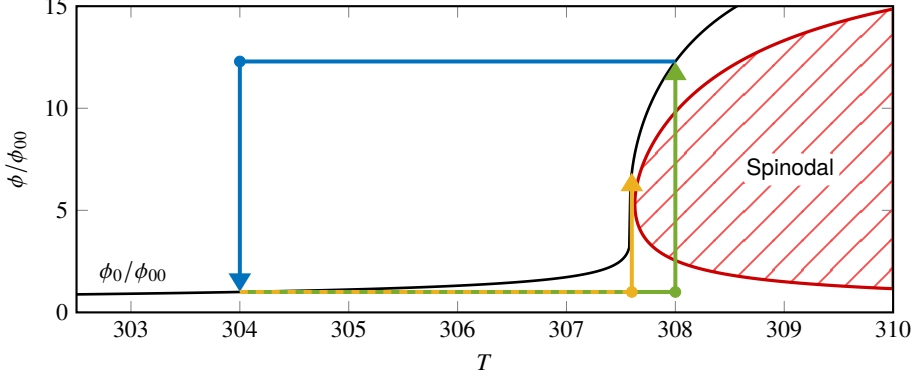
Figure 5: A plot of the region in (T, ϕ)-space where the polymer diffusivity is negative (spinodal region), alongside the equilibrium polymer fraction $\phi_0(T)$, using the gel parameters of Hirotsu *et al.* (1987) The smooth swelling problem of figure 3 is plotted in blue, with the temperature lowered and the spinodal region never approached, and the smooth drying of figure 4 is plotted in yellow. Phase separation occurs, for example, when the temperature is raised to 308 K and the path to equilibrium passes through the spinodal region, as shown in the example green trajectory.

we consider both of these effects to be forms of spinodal decomposition, with coexistence a weaker 'local' form. In either case, there are sharp differences in ϕ across very short distances, as seen especially in cases where there is significant hysteretic behaviour in the equilibrium curve (for example in the gel parameters measured by Afroze *et al.* (2000)).

Since large gradients in polymer fraction lead to large deviatoric strains, we expect that our model is unlikely to capture the dynamics of these sharp fronts exactly, since it is dependent on the assumption that these strains remain small. Attempting to replicate this behaviour regardless, through raising the temperature from 304 K to 308 K, shows that the polymer diffusivity is, in fact, negative for this case in our model. This leads to spinodal decomposition, with $D(\phi) < 0$ the criterion for such behaviour to occur. Figure 5 shows the trajectory of swelling and drying problems in (T, ϕ)-space for one particular choice of parameters, making it clear why swelling (when the temperature is lowered) never leads to negative diffusivities, and why some drying can occur (such as that of figure 4) without entering the spinodal region. In the remainder of this paper, we will consider cases of smooth drying where phase separation does not occur: indeed, taking the linear form of Π in (2.3) enforces this.

3. Response times and flow in thermo-responsive tubes

The transport equation (2.9) illustrates how the time for a gel to respond to a change in the local temperature is set by the poroelastic timescale t_{pore} for the gel, found by scaling terms in the equation to be given by

$$t_{\text{pore}} \sim \frac{\mu_l L^2}{k \Pi_{0\infty}}, \tag{3.1}$$

where L is a lengthscale for the problem. For example, in the plots of figure 3 where $L \sim a_0$, we see that a swelling sphere only attains its final radius at a time $O(\mu_l a_0^2 / k \Pi_{0\infty})$ after the temperature has been changed. In general, these timescales are slow, of the order of many hours for most macroscopic gels of interest (Webber & Worster 2023), since the response is

302 rate-limited by the permeability k, typically of the order $10^{-15}\,\mathrm{m}^2$ or smaller (Etzold *et al.*
303 2021).

304   If the physical situation we are modelling has a fixed size L, we seek an approach to
305 lower the poroelastic timescale so that the gel reacts more quickly. Recently, a new class of
306 microfluidic actuators have been designed, reliant on simple geometric designs to convert the
307 isotropic shrinkage of hydrogels above the LCST threshold into more complicated anisotropic
308 morphological changes (Maslen *et al.* 2023). Even at the micrometre scale, these devices
309 take a number of seconds to pass through a single actuation cycle, and with deswelling times
310 scaling like L^2, centimetre- or millimetre- scale devices harnessing the same physics can
311 be expected to take many hours to achieve the same shape changes. This currently confines
312 such applications to microfluidics, whilst an approach that lowers the response times could
313 find applications in actuators or soft robotics on the macroscopic scale. Recent technical
314 developments have centred on engineered structures with interconnected microchannels that
315 respond much faster to changes in temperature, but detailed modelling of these effects has
316 not been carried out (Spratte *et al.* 2022).

317   Concurrently, a number of recent advances in microfluidics have harnessed the ability of
318 hydrogels to pump fluid, either passively through their hydrophilic nature (Dong & Jiang
319 2007), or through the use of responsive hydrogels to drive peristaltic flows (Richter *et al.*
320 2009). In this latter case, fluid flows many orders of magnitude faster than the percolating
321 flow through the gel matrix can be achieved by squeezing water through microscale voids in
322 the structure. In this section, we consider the simplest such pumping device: a hollow tube of
323 thermo-responsive hydrogel filled with and surrounded by water, and how the tube responds
324 to an increase in temperature above the LCST. This provides a foundation for understanding
325 more complicated physical situations – for example, understanding the behaviour of such
326 a tube enables the modelling of a single microchannel in microporous gels, allowing for
327 quantitative modelling of response times when such gels are heated.

3.1. *Model problem*

329 We consider an infinite tube, symmetric around $z = 0$, formed from thermo-responsive gel,
330 occupying the region $a_0 < r < a_1$. The lumen of this tube is filled with water and it is
331 surrounded by water. Initially, the gel is in a swollen state with uniform polymer fraction
332 $\phi \equiv \phi_{00}$ and the temperature is constant everywhere, equal to $T_C - \Delta T$, below the critical
333 threshold for deswelling. When the temperature is brought above the critical value, the gel
334 will deswell, leading to a shrinkage of the tube, and the expulsion of water. This water can
335 be expelled radially out of the tube, carried (slowly) through the gel parallel to the axis,
336 or can be transported axially in the lumen of the tube. Though the deswelling response
337 to the temperature change is still governed by the poroelastic timescale, the tube can be
338 manufactured to be sufficiently thin that shrinkage is rapid, and bulk water can be transported
339 much more rapidly through the hollow lumen than would otherwise be the case for a solid
340 cylinder (as in the case investigated by Webber *et al.* (2023)), so that the gel device acts like
341 a small-scale displacement pump, reacting on a much faster timescale than t_{pore}.

342   The deswelling of tubes formed from hydrogels has been studied in the past, specifically in
343 the context of water-filled tubes exposed to the air, losing water through their walls as they dry
344 out (Curatolo *et al.* 2023). Qualitatively, many of the same phenomena as seen in our model
345 situation are seen here: water is driven radially from a fluid-filled pore, through the thin walls
346 of the tube, and then out into the surroundings as the gel deswells. However, notably, our
347 gels are surrounded by water and not air, so the tube is unstressed, since we are effectively
348 imposing zero external chemical potential on the outside of the tube by taking $p = 0$ here.
349 This implies that we do not expect to see the strong suction effects seen in air drying, where
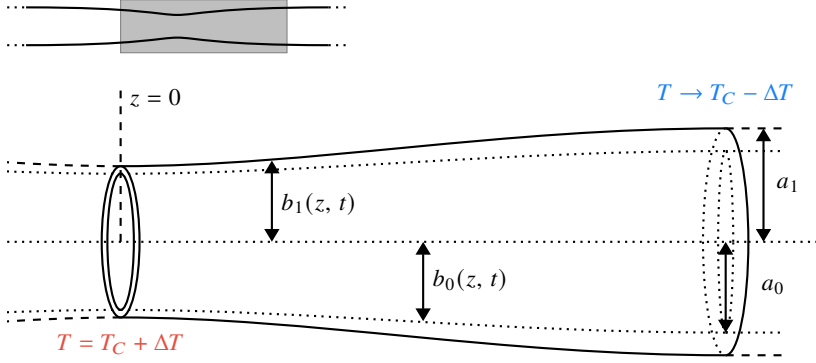350 negative inner pressures arise, which have been shown to lead to a circumferential buckling

Figure 6: An illustration of a section of the hydrogel tube in $z \geqslant 0$, occupying the region $b_0 < r < b_1$ with a hollow lumen inside. The heat pulse that starts at $z = 0$ has spread out here leading to a collapse of the tube, which is fully swollen as $z \to \infty$. At temperatures below the LCST, the tube occupies its original position $a_0 < r < a_1$.

351 instability (Curatolo *et al.* 2018). In our case, we can therefore assume that the shape of the
352 tube will remain axisymmetric for all time.
353   In order to illustrate the response of the tube to a temperature field that varies in space
354 and time, we impose a temperature $T_C + \Delta T$ at $z = 0$ for all times $t \geqslant 0$. As this heat pulse
355 spreads out $z \to \pm\infty$ in space, there is a collapse of the tube in regions with $T > T_C$, and
356 water is driven out into the surroundings and towards the still-swollen sections of tube. The
357 radius of the inner lumen is described by $r = b_0(z, t)$ whilst the outer radius is $r = b_1(z, t)$,
358 such that the collapsed tube occupies the region $b_0 < r < b_1$ and $b_i(z, 0) = a_i$ $(i = 0, 1)$.
359 Figure 6 illustrates a section of tube some time after the heat pulse has spread out from $z = 0$,
360 showing collapse behind the heat pulse front. Symmetry arguments imply that we can restrict
361 our attention to $z \geqslant 0$ in most cases, with b_0, b_1, T and ϕ all even functions of z.

362   3.2. *Deformation of the tube*
363 In line with LENS modelling, we assume that all deformation is locally isotropic, and that
364 deswelling leads to a displacement field (relative to the initial state) with axial component η
365 and radial component ξ given by

$$\frac{\xi}{r} \approx \frac{\partial \xi}{\partial r} \approx \frac{\partial \eta}{\partial z} \approx 1 - \left(\frac{\phi}{\phi_{00}} \right)^{1/3}. \tag{3.2}$$

367 Making this assumption requires the polymer fraction field to be independent of r at leading
368 order, an assumption that is reasonable to make in the slender limit of a tube with much
369 larger horizontal lengthscale than diameter. Since $\eta = 0$ at $z = 0$, owing to symmetry around
370 this point, the leading-order displacement field is

$$\xi = \left[1 - \left(\frac{\phi}{\phi_{00}} \right)^{1/3} \right] r \quad \text{and} \quad \eta = \int_0^z \left[1 - \left(\frac{\phi}{\phi_{00}} \right)^{1/3} \right] du. \tag{3.3}$$

372 Using this expression for ξ allows us to write

$$\frac{b_0}{a_0} \approx \frac{b_1}{a_1} \approx \left(\frac{\phi}{\phi_{00}} \right)^{-1/3}, \tag{3.4}$$

374 and so the local thickness of the tube is proportional to $\phi^{-1/3}$.

3.3. *Response to changes in temperature*

376 In order to derive the response of the tube to changes in temperature, it is necessary to solve
377 for the evolution of the gel composition $\phi(r, z, t)$. Initially, $\phi \equiv \phi_{00}$ everywhere and the
378 geometry of the problem shows that

$$379 \qquad \left.\frac{\partial \phi}{\partial z}\right|_{z=0} = 0 \quad \text{and} \quad \left.\frac{\partial \phi}{\partial z}\right|_{z \to \pm\infty} = 0, \tag{3.5}$$

380 arising from the symmetry of the tube and heat pulse around $z = 0$ and the assumption that
381 there is no axial flow through the tube itself (proportional to $\partial\phi/\partial z$ through equation (2.7))
382 as $z \to \pm\infty$. Indeed, we can simplify the problem further using the symmetry around $z = 0$,
383 and instead solve for the composition in $z \geqslant 0$ alone, reflecting our solution to extend to
384 negative z values.

385 There has recently been much discussion on the boundary conditions to be applied at the
386 interface of a gel with its surroundings (Xu *et al.* 2022, 2024). Significantly, it has been shown
387 that the nature of the tangential stress and velocity boundary conditions can have a significant
388 effect on the dynamics of flows within and without a hydrogel. In addition, there are potential
389 frictional effects as fluid flows cross the water–gel boundary. When flows are significant, and
390 the external fluid cannot be assumed quiescent, it is important to choose boundary conditions
391 with care, but in the present study the poroelastic timescale is sufficiently long that viscous
392 stresses are negligible (Webber & Worster 2023) and the dominant flows are radial, with only
393 small tangential components, so the external fluid is treated as a quiescent bath (even though
394 there are flows, for example, along the axis through the lumen).

395 At the surface $r = b_1(z, t)$, we assume that there is no radial stress exerted by the tube on
396 its surroundings (and vice versa), so $\sigma_{rr} = 0$. Further assuming that large-scale flows in the
397 water bath surrounding the tube are small, we take the fluid pressure to be a constant $p \equiv 0$
398 outside of the tube. Continuity of pervadic pressure then implies that $p = 0$ on $r = b_1$, and
399 this combines with the condition on σ_{rr} to give

$$400 \qquad \Pi(\phi)|_{r=b_1} = 2\mu_s \epsilon_{rr} = 0 \quad \text{so} \quad \phi(b_1(z), z, t) = \phi_0, \tag{3.6}$$

401 since the deviatoric strain is zero by our assumption of local isotropy.

402 On the inside of the tube, we cannot *a priori* make the assumption of uniform zero pervadic
403 pressure since viscous stresses arising from the lumen flows should be balanced by gradients
404 in p. As discussed in appendix B, there is an order-ε^2 correction to the interior pressure
405 field, leading to a mixed boundary condition with a contribution from $\partial\phi_2/\partial R$. However,
406 the viscous stresses are much larger on the interior of the gel than on the exterior, owing to
407 the low permeability, and it can be shown, using equation (B 7), that the lumen pressure field
408 has little effect on the gel dynamics. Thence we can use the same boundary condition on the
409 interior of the gel tube as on the exterior, taking

$$410 \qquad \phi(b_0(z), z, t) = \phi_0. \tag{3.7}$$

411 To describe the evolution of polymer fraction in time as the gel expels water, equation
412 (2.9) becomes

$$413 \qquad \frac{\partial \phi}{\partial t} + \boldsymbol{q} \cdot \boldsymbol{\nabla}\phi = \frac{1}{r}\frac{\partial}{\partial r}\left[rD(\phi,T)\frac{\partial\phi}{\partial r}\right] + \frac{\partial}{\partial z}\left[D(\phi,T)\frac{\partial\phi}{\partial z}\right] \quad \text{with}$$

$$414 \qquad D(\phi, T) = \frac{k}{\mu_l}\left[\frac{\Pi_0(T)\phi}{\phi_0(T)} + \frac{4\mu_s}{3}\left(\frac{\phi}{\phi_{00}}\right)^{1/3}\right]. \tag{3.8}$$

There is no intrinsic axial lengthscale arising from the geometry of this problem, since the tube is infinite in length, but we introduce a lengthscale L representing the characteristic distance over which temperature variations occur. In order to simplify the analysis, we make a slenderness assumption that the characteristic axial lengthscale L is much greater than the characteristic radial lengthscale a_1. Define $\varepsilon = a_1/L$, and assume that the polymer fraction field only has leading-order axial variation, with radial differences in polymer fraction being of the order $\delta \ll 1$ (arising from our assumption of local isotropy),

$$\phi = \phi_1(z, t) + \delta\phi_2(r, z, t), \tag{3.9}$$

where we have made the arbitrary choice that ϕ_2 is zero on the midline $r = [b_0(z, t) + b_1(z, t)]/2$, with ϕ_1 being the polymer fraction on the middle of the tube. Substituting this form of ϕ into the evolution equation (3.8) and separating variables, we deduce that $\delta = \varepsilon^2$. Therefore, we need only make a relatively weak slenderness assumption, since only ε^2 need be small.

The material flux $\boldsymbol{q} = q_r\hat{\boldsymbol{r}} + q_z\hat{\boldsymbol{z}}$ is solenoidal and thus $q_r/a_1 \sim q_z/L$, so $q_r \sim \varepsilon q_z$. Therefore,

$$q_r\frac{\partial\phi}{\partial r} = \varepsilon^2 q_r\frac{\partial\phi_2}{\partial r} \sim \frac{\varepsilon^3}{a_1}q_z \quad \text{and} \quad q_z\frac{\partial\phi}{\partial z} \sim \frac{\varepsilon}{a_1}q_z, \tag{3.10}$$

allowing us to neglect radial advection using this slenderness assumption. Introducing the non-dimensional variables $R = r/a_1$ and $Z = z/L$, the same non-dimensional scalings can be made to the radii b_0 and b_1, so

$$B_0 = \frac{b_0}{a_1} = \ell\left(\frac{\phi_1}{\phi_{00}}\right)^{-1/3} \quad \text{and} \quad B_1 = \frac{b_1}{a_1} = \left(\frac{\phi_1}{\phi_{00}}\right)^{-1/3}, \tag{3.11}$$

where $\ell = a_0/a_1 < 1$. The leading-order balance of equation (3.8) is thus

$$L^2\frac{\partial\phi_1}{\partial t} + Lq_z\frac{\partial\phi_1}{\partial Z} = \frac{1}{R}\left[RD(\phi_1, T)\frac{\partial\phi_2}{\partial R}\right] + \frac{\partial}{\partial Z}\left[D(\phi_1, T)\frac{\partial\phi_1}{\partial Z}\right]. \tag{3.12}$$

We now separate variables for ϕ_2, since the only term that depends on R is the first diffusive term on the right-hand side. Hence,

$$\phi_2(R, Z, t) = \frac{f(Z, T, t)}{4D(\phi_1, T)}R^2 + g(Z, T, t)\ln R + h(Z, T, t). \tag{3.13}$$

By definition, $\phi_2 = 0$ on the midline of the tube $R = (B_0 + B_1)/2$ and $\phi_2 = [\phi_0(T) - \phi_1]/\varepsilon^2$ on $R = B_0$ and $R = B_1$ from boundary conditions (3.6) and (3.7), so ϕ_2 is symmetric around the midline, with

$$\phi_2(R, Z, t) = \frac{4[\phi_0(T) - \phi_1]}{\varepsilon^2(1-\ell)^2}\left(\frac{\phi_1}{\phi_{00}}\right)^{2/3}\left[R - \frac{1+\ell}{2}\left(\frac{\phi_1}{\phi_{00}}\right)^{-1/3}\right]^2 \quad \text{with}$$

$$f = \frac{16D(\phi_1, T)[\phi_0(T) - \phi_1]}{\varepsilon^2(1-\ell)^2}\left(\frac{\phi_1}{\phi_{00}}\right)^{2/3}. \tag{3.14}$$

This allows us to deduce the radial structure of the polymer fraction given the value of ϕ_1, the polymer fraction on the inside of the tube. This is found by solving the evolution equation (3.12), which is now fully-determined up to the total axial flux. Using the approach outlined

448 in Webber *et al.* (2023),

$$
L q_z = \frac{D(\phi_1, T)}{\phi_1} \frac{\partial \phi_1}{\partial Z} + L \left(\frac{\phi_1}{\phi_{00}} \right)^{-1/3} \frac{\partial \eta}{\partial t}
$$

$$
= \frac{D(\phi_1, T)}{\phi_1} \frac{\partial \phi_1}{\partial Z} - \frac{L^2}{3} \left(\frac{\phi_1}{\phi_{00}} \right)^{-1/3} \int_0^Z \left(\frac{\phi_1}{\phi_{00}} \right)^{-2/3} \frac{\partial \phi_1}{\partial t} \, du. \tag{3.15}
$$

451 This, alongside the form of ϕ_2 from equation (3.14), can then be substituted into equation
452 (3.12), which we non-dimensionalise by introducing the variables

$$
\tau = \frac{k \Pi_{00} t}{\mu_l L^2}, \quad \Phi_{0,1,2,\infty} = \frac{\phi_{0,1,2,0\infty}}{\phi_{00}}, \quad \mathcal{M} = \frac{\mu_s}{\Pi_{00}}, \quad \mathcal{D}(\Phi_1, T) = \frac{\mu_l}{k \Pi_{00}} D(\phi_1, T). \tag{3.16}
$$

454 Then,

$$
\frac{\partial \Phi_1}{\partial \tau} + \frac{\mathcal{D}}{\Phi_1} \left(\frac{\partial \Phi_1}{\partial Z} \right)^2 - \frac{\Phi_1^{-1/3}}{3} \frac{\partial \Phi_1}{\partial Z} \int_0^Z \Phi_1^{-2/3} \frac{\partial \Phi_1}{\partial \tau} \, du = \mathcal{F} + \frac{\partial}{\partial Z} \left[\mathcal{D} \frac{\partial \Phi_1}{\partial Z} \right] \quad \text{with}
$$

$$
\mathcal{D} = \frac{\Pi_0(T)}{\Pi_{00}} \frac{\Phi_1}{\Phi_0(T)} + \frac{4\mathcal{M}}{3} \Phi_1^{1/3} \quad \text{and} \quad \mathcal{F} = \frac{16 \Phi_1^{2/3} \mathcal{D}[\Phi_0(T) - \Phi_1]}{\varepsilon^2 (1 - \ell)^2}. \tag{3.17}
$$

457 This is to be solved subject to the initial condition $\Phi_1 \equiv 1$ and subject to boundary conditions
458 $\partial \Phi_1 / \partial Z = 0$ at both $Z = 0$ and as $Z \to \infty$. In the present study, a finite-difference scheme
459 akin to that summarised in the supplementary material of Webber *et al.* (2023) is used to
460 solve equation (3.17). From this solution, equation (3.14) gives the radial polymer fraction
461 structure, and the shape of the tube is given by

$$
\ell \Phi_1^{-1/3} \leqslant R \leqslant \Phi_1^{-1/3}, \tag{3.18}
$$

463 at leading order in the small parameter ε^2. The form of the function $\mathcal{F}$ implies that, for our
464 model to be consistent, Φ_1 must everywhere be close to the piecewise-constant equilibrium
465 polymer fraction Φ_0, or else our scaling arguments for the terms in the advection-diffusion
466 equation will be invalid. We can check this assumption after calculating the solution to verify
467 the validity of our modelling.

3.4. *Response to uniform temperature change*

469 Before studying the response of a hollow tube to a propagating heat pulse, we first consider
470 the case where the temperature is everywhere brought up from below the LCST to $T_C + \Delta T$
471 at $t = 0$. The response of the tube is axially-uniform, evolving following a simplified form of
472 equation (3.17),

$$
\frac{\partial \Phi_1}{\partial \tau} = \frac{16(\Phi_\infty - \Phi_1)}{\varepsilon^2 (1 - \ell)^2} \left(\tilde{\Pi} \frac{\Phi_1^{5/3}}{\Phi_\infty} + \frac{4\mathcal{M}}{3} \Phi_1 \right), \tag{3.19}
$$

474 where $\tilde{\Pi} = \Pi_{0\infty} / \Pi_{00}$. We can use this equation to understand how the material parameters
475 Φ_∞, $\mathcal{M}$ and $\tilde{\Pi}$ affect the response time to a change in temperature without the added
476 complication of spatial variations. We know that the polymer fraction on the interior of the
477 tube wall will approach Φ_∞ as time goes on, with the outside polymer fraction instantaneously
478 reaching this value, but the rate at which this steady state is approached may vary. To measure
479 the rate of deswelling, define the deswelling timescale τ_{99} as the time taken for

$$
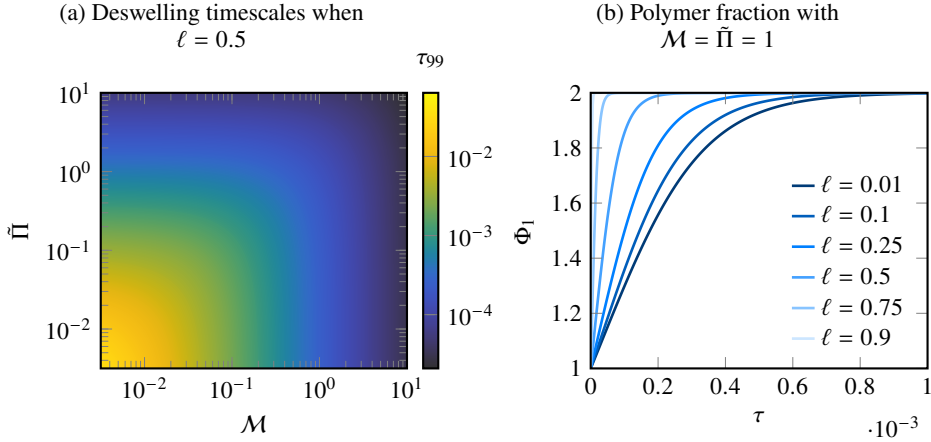\Phi_1 \geqslant \Phi^* - \frac{\Phi^* - 1}{100}. \tag{3.20}
$$

Figure 7: Plots of the one-dimensional deswelling of a tube when the temperature is uniformly changed when $\Phi_\infty = 2$ and $\varepsilon = 0.1$. This shows the variation of the deswelling timescale τ_{99} (the time taken for $\Phi_1 \geqslant 1.99$) and the approach to steady state for a number of tube thicknesses.

Straightforwardly, it is clear that deswelling is more rapid when there is a greater contrast between ϕ_{00} and $\phi_{0\infty}$, since the bracketed term $\Phi_\infty - \Phi_1$ is greater in magnitude. Thus, gels with more dramatic deswelling will approach their steady states faster. Figure 7a shows how the time taken to reach Φ_∞ depends on the stiffness of the gel (encoded by $\mathcal{M}$) and the relative strength of the osmotic pressure at higher temperatures (encoded by $\tilde{\Pi}$). Stiffer gels resist the formation of deviatoric strains, which arise from differences in polymer fraction, so the interior must deswell to catch up with the outside of the tube, leading to a much faster deswelling process as $\mathcal{M}$ increases. Similarly, larger values of $\tilde{\Pi}$ lead to more rapid interstitial flows driven by pervadic pressure gradients, and so the time to deswell decreases as $\tilde{\Pi}$ increases.

Figure 7b illustrates the approach of the polymer fraction on the interior of the tube wall, Φ_1, to the equilibrium value Φ_∞, showing how the approach is more rapid for thinner tubes where there is a shorter distance for water to diffuse out.

3.5. *Heat transfer in the system*

If, instead of a uniform temperature field, we impose a fixed temperature $T = T_C + \Delta T$ at $Z = 0$, we expect this heat pulse to spread out in the axial direction, symmetrically around the origin, with a deswelling front behind which $T > T_C$, and in front of which $T < T_C$. Modelling the transport of heat through the water, gel scaffold, and within the pore space water, is a potentially complicated task, and a number of different transport processes must be accounted for, as well as the energetic contributions of swelling, deswelling and deformation (Kaviany 1995). In the present study, we will consider the simplest possible case, acknowledging that more complicated phenomena such as dispersion will also contribute to heat transfer, but can be reasonably neglected on the assumption that flows through the gel are sufficiently slow.

There is much discussion in the literature of thermoelasticity with specific applications to hydrogels (Cai & Suo 2011; Drozdov 2014; Brunner *et al.* 2024), and here we take a necessarily simpler model, justifying why deformation and swelling do not contribute to temperature evolution at leading order. In appendix C, we derive a temperature evolution

508 equation for a gel in the LENS formalism in the absence of external heat supply ($R = 0$),

$$509 \quad \frac{\partial T}{\partial t} + \boldsymbol{q} \cdot \boldsymbol{\nabla} T = \kappa \nabla^2 T + \frac{k(\phi)}{\rho c \mu_l} |\boldsymbol{\nabla} p|^2 + \frac{1}{\phi} \left(\frac{\Pi(\phi)}{\rho c} + T \right) \left(\frac{\partial \phi}{\partial t} + \boldsymbol{q} \cdot \boldsymbol{\nabla} \phi \right), \quad (3.21)$$

510 where c is the specific heat capacity, ρ is the gel density and κ is a spatially-averaged
511 thermal diffusivity. In the water surrounding the hydrogel, heat transfer is described by the
512 advection-diffusion equation

$$513 \quad \frac{\partial T}{\partial t} + \boldsymbol{u} \cdot \boldsymbol{\nabla} T = \boldsymbol{\nabla} \cdot (\kappa_w \boldsymbol{\nabla} T) = \kappa_w \nabla^2 T, \quad (3.22)$$

514 where κ_w is the thermal diffusivity of water, assumed to be spatially-uniform. In our model,
515 we assume that $\kappa \approx \kappa_w$. Certainly this is true in regions where $\phi \ll 1$ and the gel remains
516 swollen, since the contributions of diffusivity in the solid are limited here, a statement
517 supported by experiment and molecular dynamics simulation (Xu *et al.* 2018). In deswollen
518 regions where the polymer fraction is larger, κ is likely of the same order of magnitude as
519 κ, since the thermal diffusivity of polymer chains is of the same magnitude as the thermal
520 diffusivity of water (Freeman *et al.* 1987). However, such regions are a small fraction of the
521 total spatial domain, and the fact that the collapsed tube is thin here means that we neglect
522 any variation from κ_w in this region.
523   There are two potential timescales in the heat transfer problem in the gel – the poroelastic
524 timescale t_{pore} of equation (3.1), and the thermal timescale $t_{\text{therm}} = L^2/\kappa$. Their ratio is

$$525 \quad \frac{t_{\text{pore}}}{t_{\text{therm}}} = \frac{\kappa}{D} = Le, \quad (3.23)$$

526 the Lewis number, representing the ratio of thermal to compositional diffusivities. In the case
527 $Le \gg 1$, equation (3.21) simply reduces to the diffusion equation, since all but the first term
528 on the right-hand side depend on the (slow) reconfiguration of the gel scaffold.
529   We know that flow and deformation of the gel is mediated by the low permeability of
530 the polymer scaffold, with $k \sim 10^{-15} \text{ m}^2$, and therefore expect that the transfer of heat
531 by conduction will occur much faster than changes in shape to the gel. The compositional
532 diffusivity $k\Pi_{00}/\mu_l$ typically scales like $10^{-8} \text{ m}^2\text{s}^{-1}$, whilst $\kappa \sim 10^{-7} \text{ m}^2\text{s}^{-1}$, so $Le \sim 10$.
533 In the present study, we restrict our attention to the large-Le limit for simplicity, where heat
534 transfer in both the gel and water can be modelled by

$$535 \quad \frac{\partial \theta}{\partial \tau} = Le \frac{\partial^2 \theta}{\partial Z^2} \quad \text{with} \quad \begin{cases} \theta(0, \tau) = 1, \\ \theta \to -1 & \text{as } Z \to \infty \end{cases} \quad (3.24)$$

536 where $\theta = (T - T_C)/\Delta T$. There are reasonable physical situations where these assumptions
537 do not apply, but we do not consider them here – modelling such cases would require a careful
538 consideration of heat transfer by advection, dispersion and diffusion, as well as incorporating
539 the effect of fast fluid flows into boundary conditions at the gel surface (Xu *et al.* 2022).
540 Equation (3.24) has a solution in terms of the error function, with

$$541 \quad \theta = 2 \operatorname{erfc} \left(\frac{Z}{2\sqrt{Le\,\tau}} \right) - 1, \quad (3.25)$$

542 where erfc is the complementary error function (Abramowitz & Stegun 1970). In order to
543 understand the response of the gel to the diffusive heat pulse, we first seek the position of the
544 deswelling front $Z = Z_C$ where $\theta = 0$. This is found using equation (3.25), with

$$545 \quad \operatorname{erfc} \left(\frac{Z_C}{2\sqrt{Le\,\tau}} \right) = \frac{1}{2} \quad \text{so} \quad Z_C = 2 \operatorname{erfc}^{-1} \left(\frac{1}{2} \right) \sqrt{Le\,\tau} \approx 0.9539\sqrt{Le\,\tau}. \quad (3.26)$$

Parameter	Value
Deswollen scaled polymer fraction Φ_∞	2
Ratio of osmotic pressure scales $\tilde{\Pi}$	1
Aspect ratio $\varepsilon = a_1/L$	0.1
Shear parameter $\mathcal{M}$	1
Lewis number Le	10

Table 1: Parameter values used in the modelling of drying tubes from section 3.6 onwards, with the effect of changing Φ_∞, $\tilde{\Pi}$ and $\mathcal{M}$ discussed in section 3.4.
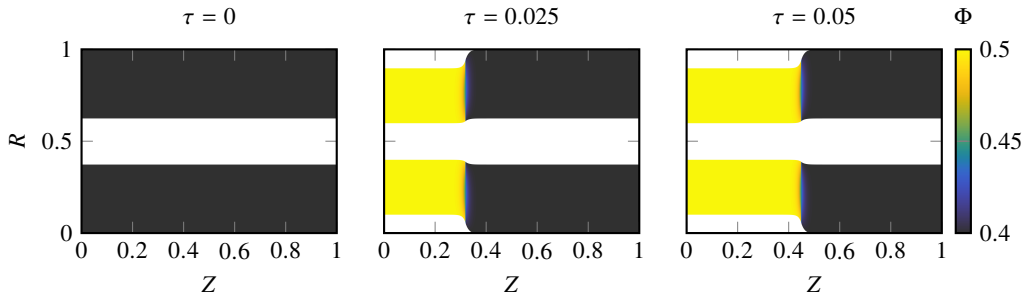

Figure 8: Plots of the evolution of a hollow thermo-responsive hydrogel tube with parameters from table 1 and $\ell = 0.25$. The heat pulse diffuses from left to right, with the gel shrinking behind it.

3.6. *Response to pulses of heat*

Using the model summarised in equation (3.17), we can compute the mechanisms by which a thermo-responsive gel tube will collapse in response to a temporally– and spatially-varying temperature field (3.25). Key to the behaviour here is the fact that heat diffuses on a faster timescale than the water can diffuse through the polymer, leading to a smooth front centred on the pulse front $Z_C(\tau)$. From this point onwards, we will use the parameters in table 1 in all modelling, having discussed the effect of varying $\mathcal{M}$ and $\tilde{\Pi}$ on the one-dimensional deswelling in previous sections. Figure 8 shows the thickness of a tube at different times as heat diffuses and the gel shrinks. Notice that the shrinkage, though rapid, is not instantaneous in time, since the slow diffusion of water out of the walls of the tube sets a delayed response.

In order for the gel to deswell, water must flow from the walls of the tube into the surrounding water, the lumen at the centre of the tube, or through the gel itself parallel to the axis. Clearly, if the walls of the tube are thinner, driving water from the hydrogel is more rapid, since the water has less of a distance to diffuse outwards, and we expect a more rapid response to changes in temperature for larger values of ℓ. The more rapid approach to steady state is shown in figure 9a, where the sharper equilibrium profile is approached more closely around the drying front $Z_C(\tau)$ for thinner tube walls. Assuming that the radial fluxes are locally dominant, equation (3.17) reduces to the one-dimensional case of section 3.4,

$$\frac{\partial \Phi_1}{\partial \tau} \approx \frac{16\Phi_1^{2/3}\mathcal{D}}{\varepsilon^2(1-\ell)^2} \times \begin{cases} \Phi_\infty - \Phi_1 & Z < Z_C \\ 1 - \Phi_1 & Z > Z_C \end{cases}, \tag{3.27}$$

away from the front at $Z = Z_C$ (where $\partial\Phi_1/\partial Z$ will be significant). Then, timescales decrease like $(1 - \ell)^2$ when ℓ is increased. In the opposite limit as $\ell \to 0$, adjustment happens on the unmodified poroelastic timescale.

(a) Relaxation to the equilibrium
polymer fraction around Z_C

(b) Fitted values of $A(\ell)$ showing
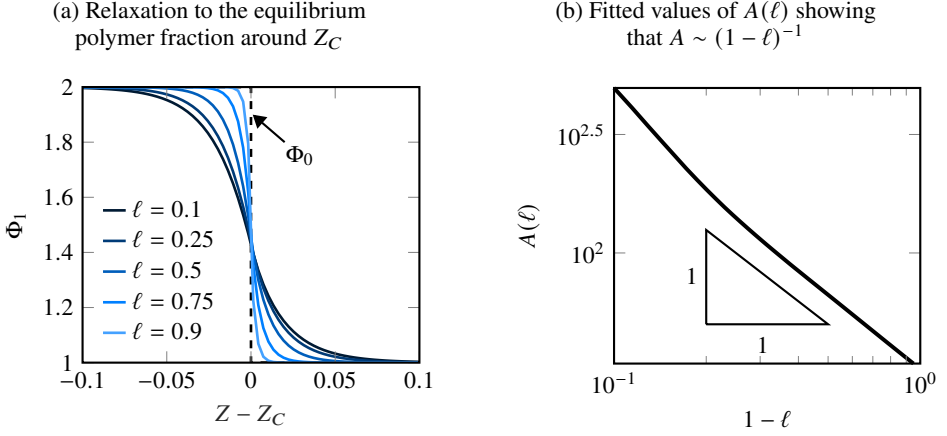that $A \sim (1 - \ell)^{-1}$

Figure 9: Plots of the interior polymer fraction Φ_1 at $\tau = 10^{-2}$ with the same parameters as in figure 8, showing how the relaxation to the steady state $\Phi = \Phi_0(T)$ around the drying front $Z = Z_C(\tau)$ is much faster for thinner tubes $\ell \to 1$. These profiles can be approximated by a tanh function, as in equation (3.28), with fitting parameter $A(\ell)$ shown in the logarithmic plot on the right.

568 From figure 8, it is clear that the structure of the solution around $Z = Z_C(\tau)$ appears to
569 propagate like a travelling wave centred on the deswelling front, since the contribution of
570 axial flows through the gel is limited compared to that of radial flows. Therefore, we can
571 consider the quasi-one-dimensional problem in the new coordinate $Z - Z_C$. The plots in
572 figure 9 suggest that polymer fraction can locally be approximated by a smooth step around
573 $Z = Z_C(\tau)$, with the steepness a function of thickness ℓ. We thus propose that

574
$$\Phi_1 \approx \Phi_\infty - \frac{\Phi_\infty - 1}{2} \left\{ 1 + \tanh\left[A(\ell)\left(Z - Z_C\right)\right] \right\}, \tag{3.28}$$

575 for some scaling factor A, a function of ℓ, representing the sharpness of the drying front.
576 Figure 9 shows that $A(\ell) \sim (1 - \ell)^{-1}$, and therefore the thickness of the adjustment region
577 around the front $Z = Z_C(\tau)$ scales like $(1 - \ell)$.

578 3.6.1. *Flow through the walls*

579 Flow in the walls of the tube is driven by diffusive transport of water from more swollen
580 regions to drier regions, with an interstitial fluid velocity

581
$$\boldsymbol{u_g} = \frac{D(\phi)}{\phi}\boldsymbol{\nabla}\phi = \frac{k\Pi_{00}}{\mu_l}\left(\frac{1}{L}\frac{\partial \Phi_1}{\partial Z}\hat{z} + \frac{\varepsilon^2}{a_1}\frac{\partial \Phi_2}{\partial R}\hat{r}\right) \times \begin{cases} \dfrac{\tilde{\Pi}}{\Phi_\infty} + \dfrac{4\mathcal{M}}{3}\Phi_1^{-2/3} & Z < Z_C \\[2ex] 1 + \dfrac{4\mathcal{M}}{3}\Phi_1^{-2/3} & Z > Z_C \end{cases}, \tag{3.29}$$

582 at leading order in the aspect ratio. We define a dimensionless radial fluid velocity U_g scaled
583 with a_1 divided by the poroelastic timescale and an axial velocity V_g scaled with L divided
584 by the same timescale, so that

585
$$\left(V_g, U_g\right) = \left(\frac{\partial \Phi_1}{\partial Z}, \frac{\partial \Phi_2}{\partial R}\right) \times \begin{cases} \dfrac{\tilde{\Pi}}{\Phi_\infty} + \dfrac{4\mathcal{M}}{3}\Phi_1^{-2/3} & Z < Z_C. \\[2ex] 1 + \dfrac{4\mathcal{M}}{3}\Phi_1^{-2/3} & Z > Z_C. \end{cases} \tag{3.30}$$
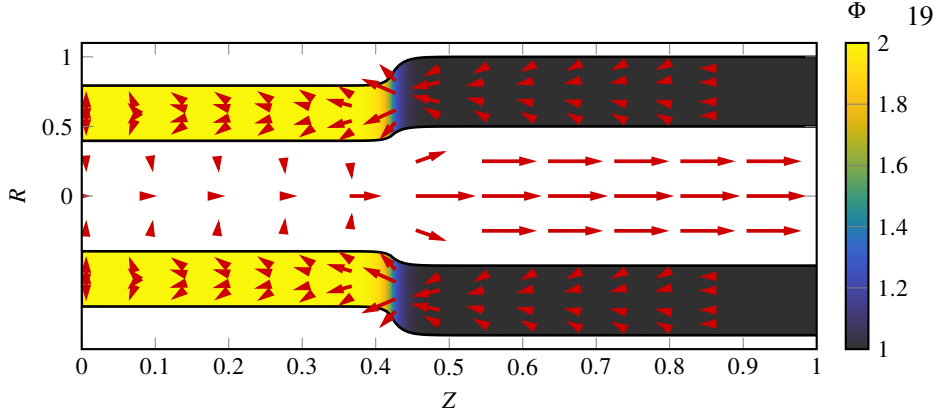
Figure 10: A plot at $\tau = 0.02$ of a drying gel tube with the same parameters as in figure 8. The colours represent the polymer fraction field, with arrows in the gel showing the direction and magnitude of the interstitial flow field $\boldsymbol{u_g}$, as defined in equation (3.29). The arrows within the lumen show the flow within the tube, with the form of equation (3.34).
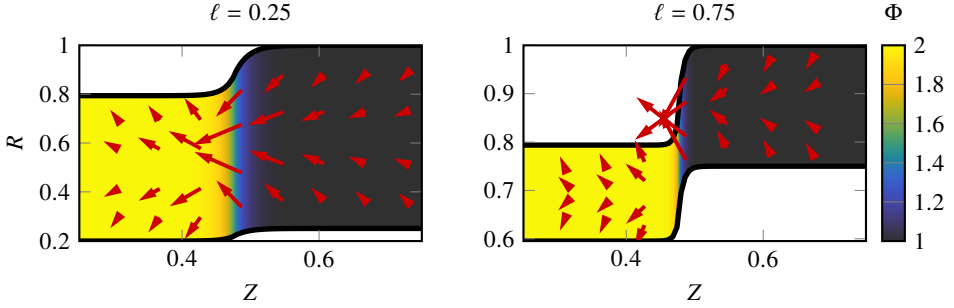

Figure 11: Plots close to $Z = Z_C(\tau)$ when $\tau = 0.025$, illustrating dominant radial flows when the gel is thinner ($\ell = 0.75$) versus the thicker ($\ell = 0.25$) gel. In all other regards, the parameters are the same as in figure 10. Notice the directional change either side of the drying front.

Figure 10 illustrates an example flow field through the walls of the gel, with flow from more swollen to less swollen regions. In the dried region behind the temperature front, radial fluxes are outwards as water is driven out of the shrinking gel, with fluid transported axially towards the drier regions to the left. In $Z > Z_C$, however, fluxes are inwards towards the gel. In order to understand why this is, notice that the gel is more swollen on its interior than exterior when $Z < Z_C$ (as the tube fully dries from the outside in) and more swollen on its exterior than interior when $Z > Z_C$ (as the tube is fully swollen on $R = B_1$ with some loss of fluid in the interior due to axial fluxes towards the drier tube). Hence, there needs to be water drawn in from the surrounding fluid to replenish these regions.

In general, therefore, the tube draws water inwards ahead of the deswelling front, and then expels the water behind this front. This is shown in detail in figure 11, where the dominance of radial fluxes in thinner gel layers is also clear.

3.6.2. *Flow in the lumen*

There is also a flow of water through the lumen of the tube, resulting from mass conservation and the redistribution of fluid as the tube dries out. Assuming that the flow within the tube lumen can be described by a Stokes flow $\boldsymbol{v} = v_r\hat{\boldsymbol{r}} + v_z\hat{\boldsymbol{z}}$ with viscosity μ_l,

$$\mu_l\nabla^2\boldsymbol{v} - \boldsymbol{\nabla}p = \boldsymbol{0} \quad \text{and} \quad \boldsymbol{\nabla}\cdot\boldsymbol{v} = 0. \tag{3.31}$$

Using the slenderness approximation and assuming that pervadic pressure is independent of r, axial derivatives can be neglected in the radial component of the momentum equation, and it is found that the radial component of the velocity must be linear in r if it is to be regular at $r = 0$, and so

$$v_r = C(z)r \quad \text{and} \quad v_z = -2 \int_0^z C(z') \, dz', \tag{3.32}$$

assuming that $v_z = 0$ at $z = 0$ by symmetry. We then non-dimensionalise to find a radial velocity U scaled with a_1 divided by the poroelastic timescale, and an axial velocity V scaled with L divided by the poroelastic timescale. The radial velocities in the gel are given by

$$U_g = \frac{8\Phi_1^{2/3} \mathcal{D}(\Phi_1) \left[\Phi_0(T) - \Phi_1 \right]}{\varepsilon^2 (1 - \ell)^2} \left(R - \frac{1 + \ell}{2} \Phi_1^{-1/3} \right), \tag{3.33}$$

and therefore, matching velocities at $R = \ell \Phi_1^{-1/3}$,

$$U = -\frac{4\Phi_1 \mathcal{D} \left[\Phi_0(T) - \Phi_1 \right]}{\varepsilon^2 (1 - \ell)^2} R \quad \text{and} \quad V = \frac{8}{\varepsilon^2 (1 - \ell)^2} \int_0^Z \Phi_1 \mathcal{D} \left[\Phi_0(T) - \Phi_1 \right] \, dZ'. \tag{3.34}$$

Behind the temperature front, flow is radially inwards, since the gel dries into its interior, and this drives a forwards flow along the tube by mass conservation. The magnitude of this flow decreases ahead of the front as there is a weak outward radial flow here.

We can gain some insight into the nature of the axial fluid transport V by considering the fitted form of equation (3.28), from which we can calculate the evolution of velocity in time. Figure 12 shows how fluid, stationary far behind the temperature front, is driven in the same direction as the thermal front, with a maximum axial velocity $V_{\max}$ at $Z = Z_C(\tau)$. The velocity the decays to a constant value in the tube ahead of the front, which is nonzero by mass conservation. Figure 12b shows that the height of this axial flow pulse scales like $A(\ell)^{-1} \sim 1 - \ell$. Since the thickness of this adjustment region scales like $A(\ell)$, the height of the pulse increases with ℓ, but its width decreases with ℓ, such that the total flux carried by the pulse is constant as ℓ is varied.

3.7. *Summary of results*

In this section, we have used the conceptually simple model for a responsive tubular pump to illustrate a number of results attainable using the responsive LENS formalism that can then be applied to the design of more complicated responsive hydrogel devices. First, we illustrated how the relative impermeability of hydrogels allows for the gel dynamics problem to be decoupled from the fluid flow within cavities (in this example, the lumen of the gel tube), so that the induced pumping flows can be straightforwardly deduced as an output of our modelling, as justified in appendix B. This allowed us to construct an explicit model for the deswelling of responsive gels as the temperature is changed, quantifying exactly how this deswelling is more rapid for tubes that are thinner $\sim (1 - \ell)^2$ and showing how response times can be tuned by varying ℓ, the thickness parameter.

Furthermore, the assumption of slenderness and the separation of timescales between slower poroelastic deformation and faster transport of heat allows for decoupling between the thermal problem and the poroelastic problem, and so modelling the behaviour of a thermo-responsive tube to a time- and space-varying temperature field is possible in this framework. We have seen how a tube relaxes to a new equilibrium state around a thermal front, and can quantify the spatial structure of the adjustment region, which is smoother and less well-defined for thicker tubes than thinner tubes that approach the equilibrium faster. Perhaps most instructively, the LENS model gives clear expressions for the interstitial flow
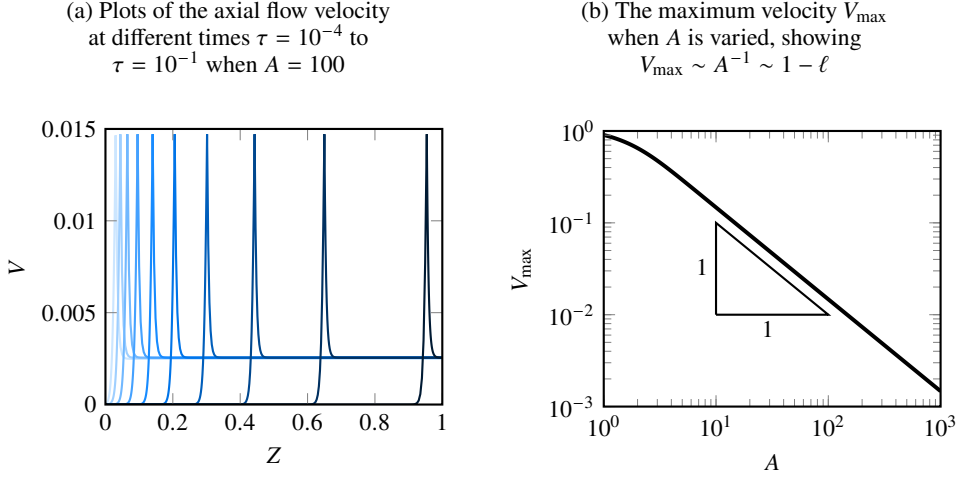
(a) Plots of the axial flow velocity at different times $\tau = 10^{-4}$ to $\tau = 10^{-1}$ when $A = 100$

(b) The maximum velocity V_{max} when A is varied, showing $V_{\text{max}} \sim A^{-1} \sim 1 - \ell$

Figure 12: Plots showing the approximate axial velocity V (computed using the form of Φ_1 in equation (3.28)) for the parameters in table 1, showing how fluid travels in a pulse from the left to the right, with the height of the pulse inversely proportional to the fit parameter $A(\ell)$.

velocities both along the axis of the tube and out of the walls, as well as the velocities within the hollow lumen, permitting predictions of the nature of the axial pumping fluxes to be made when a tube is heated from one point.

4. Conclusion

In this paper, we have extended the linear-elastic-nonlinear-swelling model outlined in Webber & Worster (2023) to incorporate a temperature-dependent osmotic pressure that can reproduce this behaviour when the temperature is brought above the LCST threshold. The approach is generic, and in some sense agnostic of the type of stimulus, and as such our model may be readily extended to, for instance, pH-responsive hydrogels.

We showed that the approach of the linear-elastic-nonlinear-swelling theory is able to reproduce the transient swelling or deswelling behaviour of thermo-responsive gels both qualitatively and quantitatively. By choosing functional forms for the osmotic pressure and shear modulus that fit the parameters used in Butler & Montenegro-Johnson (2022), we are able to use LENS to reproduce predictions from a full nonlinear Flory-Huggins approach, provided that no spinodal decomposition occurs. Our model also provides criteria for such phase separation to occur when the diffusivity – a function of macroscopic osmotic pressure and shear modulus – is negative, and dried and swollen gels can coexist adjacent to one another. In order to regularise solutions of the polymer fraction evolution equation in these cases, it is likely necessary to incorporate some kind of surface energy to penalise the formation of new surfaces (Hennessy *et al.* 2020), leading to Korteweg stresses at internal interfaces. The question of how to describe such an approach in the context of a LENS model remains a topic for future research, since the formation of sharp polymer fraction gradients is not permitted in LENS.

Some of the key applications of thermo-responsive hydrogels are hampered by the slow response times of such gels to changes in the ambient temperature. In general, hydrogel swelling or drying is a slow process, mediated by viscously-dominated interstitial flows through a low-permeability scaffold, with some gels taking hours or days to reach an equilibrium state (Bertrand *et al.* 2016). This is clearly undesirable in microfluidic devices

or actuators, and having a tunable response time to changes in temperature may be desirable for certain applications (Maslen *et al.* 2023). In order to investigate the response time of simple gel structures, we have considered the case of a hollow tube of gel that can act like a displacement pump.

In this geometry, even though the axial dimension may be large, deformation timescales are set by the diffusion of water through the thin walls, so morphological changes can occur much more rapidly than they would in a solid gel. This occurs because the shrinkage of the outside of the tube is no longer rate-limited by the need to deform and drive fluid through the interior of the gel, since water can flow relatively unimpeded down the lumen of the tube. The transport of water through the pipe-like structure that results can be used as a proxy measure of the speed of response, with water being transported large distances surprisingly quickly as a thermal signal propagates.

In order to model these tubes, we made a slenderness approximation that the polymer fraction varies axially at leading order, with only small radial corrections as water is expelled from the gel as the critical temperature threshold is exceeded. This facilitated a mathematical treatment similar to that used for transpiration through cylinders in Webber *et al.* (2023), and thus we can write down analytical expressions for all of the interstitial fluid fluxes in the gel and in the lumen. This approach permits us to tune the geometry of the tubes to match the exact response times desired, and allows for the computation of fluid flows through the pore matrix, along the axis of the tube, and out of the side walls.

Though there is no definitive measure of 'response time' in more complex geometries, we have discussed how varying the geometry and material properties of the gel that forms the tube lining can affect the speed at which fluid is transported through the lumen and the sharpness of the fluid pulse at the deswelling front. As one might expect, it is seen that thinner tubes react more rapidly to changes in temperature, and also that the resultant fluid pulse is more spatially localised around the thermal pulse in such cases. We have also elucidated the dependence of the fluid pulse driven down the pump on both the osmotic and elastic properties of the material forming the tube, enabling the design of displacement pumps with specific response characteristics.

In the future, these simple model tubes could be connected together to form a network, propagating information about external stimuli through the medium of fluid pulses much more rapidly than in a solid block of hydrogel, forming the basis for a porous sponge built from porous hydrogel, with the pore size and geometry designed to match the desired material properties. This approach has already been taken experimentally in the design of microfluidic devices that exhibit dynamic anisotropy (Maslen *et al.* 2023), and we hope that our modelling will provide potential qualitative insights into the design characteristics of such devices in the future.

Declaration of interests. The authors report no conflict of interest.

Author ORCIDs. J. J. Webber, https://orcid.org/0000-0002-0739-9574; T. D. Montenegro-Johnson, https://orcid.org/0000-0002-9370-7720

Appendix A. LENS material parameters from an energy-based approach

In Butler & Montenegro-Johnson (2022), the standard energy density function for a thermo-responsive hydrogel (Cai & Suo 2011) is used, following Flory-Huggins mixture theory and a neo-Hookean elastic model for the polymer chains,

$$\mathcal{W} = \frac{k_B T}{2\Omega_p}\left[\mathrm{tr}\left(\boldsymbol{F_d}\boldsymbol{F_d}^{\mathrm{T}}\right) - 3 + 2\ln\phi\right] + \frac{k_B T}{\Omega_f}\left[\frac{1-\phi}{\phi}\ln\left(1-\phi\right) + \chi(\phi, T)(1-\phi)\right], \quad (A\,1)$$

where $\boldsymbol{F_d}$ is the deformation gradient tensor measured relative to a fully-dry polymer. We can rewrite $\boldsymbol{F_d}$ in terms of $\boldsymbol{F}$, the deformation gradient measured relative to a state where $\phi \equiv \phi_{00}$, since the transition between the two states can be described by an isotropic scaling transformation,

$$\boldsymbol{F_d} = \left(\phi_{00}^{-1/3}\boldsymbol{I}\right)\boldsymbol{F} = \phi_{00}^{-1/3}\boldsymbol{F} \quad \text{so} \quad \mathrm{tr}\left(\boldsymbol{F_d}\boldsymbol{F_d}^{\mathrm{T}}\right) = \phi_{00}^{-2/3}\mathsf{F}_{ab}\mathsf{F}_{ab}, \quad (A\,2)$$

using Einstein summation convention. Following the approach of Cai & Suo (2012), the Terzaghi effective stress tensor $\sigma^{(e)}$ (i.e. $\sigma + p\boldsymbol{I}$) has components given by

$$\sigma_{ij}^{(e)} = \phi\frac{\partial \mathcal{W}}{\partial \mathsf{F}_{ik}}\mathsf{F}_{jk}, \quad (A\,3)$$

again using summation convention. This derivation is based on the classical approach by Coleman & Noll (1963), coupling a local entropy imbalance law with the expression for the rate of change of internal energy (Brunner *et al.* 2024). Since $\det \boldsymbol{F} = \phi_{00}/\phi$, the expression for the derivative of a determinant with respect to a matrix (Petersen & Pedersen 2012) implies that

$$\frac{\partial \phi}{\partial \mathsf{F}_{ik}} = -\phi\mathsf{F}_{ki}^{-1}. \quad (A\,4)$$

Hence,

$$\frac{\partial \mathcal{W}}{\partial \mathsf{F}_{ik}} = \frac{k_B T}{\Omega_f}\left\{\frac{1}{\Omega\phi_{00}^{2/3}}\mathsf{F}_{ik} + \left[\frac{\ln\left(1-\phi\right)}{\phi} + 1 + \phi\chi(\phi, T) - \phi(1-\phi)\frac{\partial\chi}{\partial\phi} - \frac{1}{\Omega}\right]\mathsf{F}_{ki}^{-1}\right\} \quad \text{and}$$

$$\sigma_{ij}^{(e)} = \frac{k_B T}{\Omega_f}\left\{\left[\ln\left(1-\phi\right) + \phi + \phi^2\chi - \phi^2(1-\phi)\frac{\partial\chi}{\partial\phi} - \frac{\phi}{\Omega}\right]\delta_{ij} + \frac{\phi}{\Omega\phi_{00}^{2/3}}\mathsf{F}_{ik}\mathsf{F}_{jk}\right\}, \quad (A\,5)$$

where $\Omega = \Omega_p/\Omega_f$ represents the volume of polymer molecules relative to solvent molecules. Separating the deformation gradient into an isotropic part due to swelling and shrinkage and a deviatoric part that can be related to deviatoric Cauchy strain ϵ (Webber & Worster 2023),

$$\mathsf{F}_{ik}\mathsf{F}_{jk} = \left(\frac{\phi}{\phi_{00}}\right)^{-2/3}\delta_{ij} + \frac{2\phi_{00}}{\phi}\epsilon_{ij}, \quad (A\,6)$$

and so the two temperature-dependent material parameters are

$$\Pi(\phi) = \frac{k_B T}{\Omega_f}\left[\Omega^{-1}\left(\phi - \phi^{1/3}\right) - \phi - \ln\left(1-\phi\right) - \phi^2\chi + \phi^2(1-\phi)\frac{\partial\chi}{\partial\phi}\right] \quad \text{and} \quad (A\,7a)$$

$$\mu_s(\phi) = \frac{k_B T\phi_{00}^{1/3}}{\Omega_p}. \quad (A\,7b)$$

Notice that the shear modulus is independent of polymer fraction, and increases with temperature and chain length (longer polymer chains have a larger Ω_p). The temperature-

Model	A_0	A_1	B_0	B_1	Ω
ANB (Afroze *et al.* 2000)	−12.947	17.92	$0.04496\,\mathrm{K}^{-1}$	$-0.0569\,\mathrm{K}^{-1}$	100
HHT (Hirotsu *et al.* 1987)	−62.22	−58.28	$0.20470\,\mathrm{K}^{-1}$	$0.19044\,\mathrm{K}^{-1}$	720

Table 2: Fitted parameter values for the two thermo-responsive hydrogels considered in Butler & Montenegro-Johnson (2022), based on two pre-existing models from the literature.
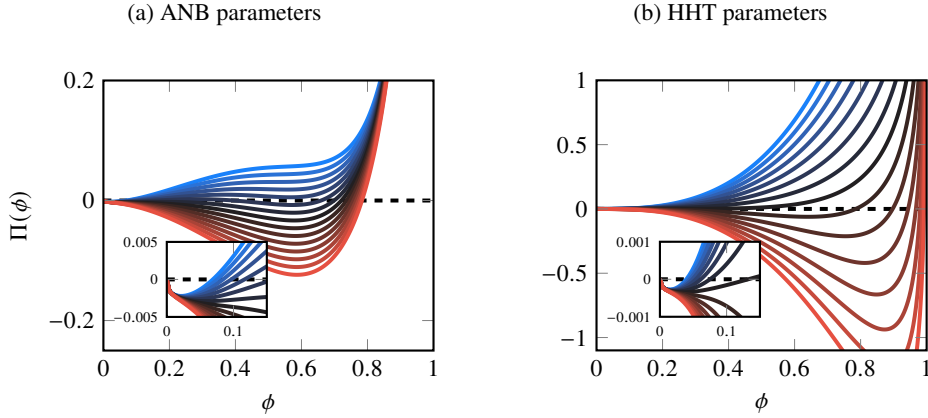

Figure 13: Plots of the osmotic pressure (A 7*a*) for the two choices of fitted parameters in table 2 as the temperature is raised from 300 K (below T_C) to 315 K (above T_C) (red). Notice the change in equilibrium polymer fraction as the threshold is crossed.

dependence of the osmotic pressure is more complicated, with contributions from the $k_B T$ prefactor, χ, and $\partial \chi / \partial \phi$.

To incorporate temperature dependence in $\chi(\phi, T)$, Butler & Montenegro-Johnson (2022) specify an interaction parameter that depends linearly on both ϕ and T,

$$\chi(\phi, T) = A_0 + B_0 T + (A_1 + B_1 T)\phi, \tag{A 8}$$

where the four parameters can be fitted to existing models in the literature. Here, we consider two example models – the first is based on Afroze *et al.* (2000) (ANB), and the second is based on Hirotsu *et al.* (1987) and henceforth referred to as HHT. The fitting parameters, as found in Butler & Montenegro-Johnson (2022), are summarised in table 2. Figure 13 shows plots of the osmotic pressure in the case of these two parameter choices, showing (slightly) negative values of Π as $\phi \to 0$ corresponding to states with a propensity to deswell, and $\Pi \to \infty$ as $\phi \to 1$, illustrating very dry states with a propensity to swell. As the temperature is increased, the location of equilibrium states changes.

To find these equilibrium polymer fractions, we set $\Pi = 0$ and thus consider the expression

$$\Omega^{-1}\left(\phi_0 - \phi_0^{1/3}\right) - \phi_0 - \ln\left(1 - \phi_0\right) - \phi_0^2\left[A_0 + B_0 T + (2\phi_0 - 1)(A_1 + B_1 T)\right] = 0, \tag{A 9}$$

for the two choices of parameters, and figure 14 shows the variation of ϕ_0 with temperature in both the ANB and HHT parameter sets. In the case of the parameters of Afroze *et al.* (2000), it is especially apparent that there are two critical temperatures. As the temperature is lowered from around 310 K, and the equilibrium polymer fraction ϕ_0 decreases (swelling), there is a rapid increase in swelling at $T_C^{\uparrow} \approx 304.5\,\mathrm{K}$, the swelling critical temperature.
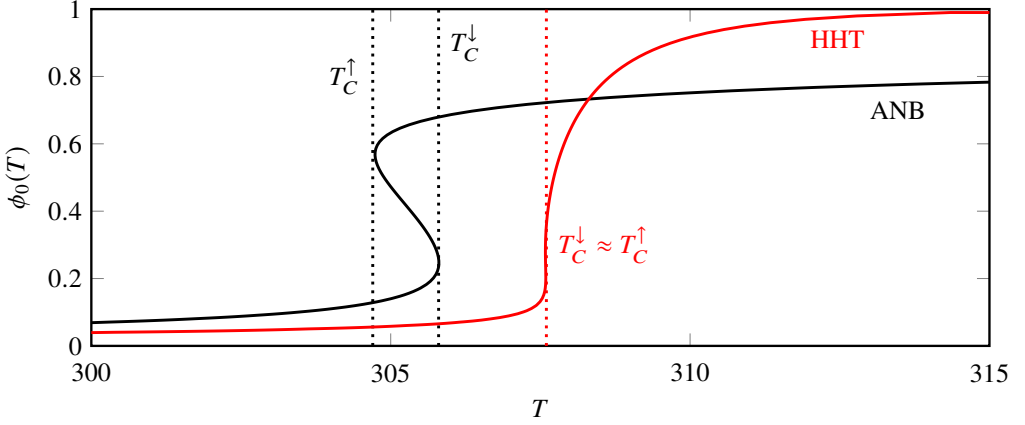
Figure 14: Plots of the equilibrium polymer fraction, determined by $\Pi(\phi_0) = 0$ in equation (A 9). Two choices of parameter values are plotted; those determined by Afroze *et al.* (2000) (ANB) and Hirotsu *et al.* (1987) (HHT), showing the volume phase transition temperatures for swelling ($T_C^\uparrow$) and shrinking ($T_C^\downarrow$), respectively.

As the temperature is increased from around 300 K, however, there is a different critical temperature, $T_C^\downarrow \approx 306$ K at which there is rapid drying. This hysteresis is in fact exhibited in the case of both sets of parameters, where there are multiple solutions in a narrow band of temperatures around the critical volume phase transition temperature T_C, an effect which we ignore in the present study, modelling the equilibrium polymer fraction as single-valued at any temperature.

In the low-temperature (i.e. swollen) states, we further assume that $\phi_0 \ll 1$, so the leading-order balance of equation (A 9) is

$$\phi_0 \approx \left[\Omega \left(\frac{1}{2} - (A_0 - A_1) - (B_0 - B_1)T \right) \right]^{-3/5}, \tag{A 10}$$

equal to the classical approximation in gels that are not thermo-responsive (Doi 2009; Webber & Worster 2023). In both of the models, this gives $\phi_0 \sim 0.01$ for sufficiently low temperatures, but there is a singularity at

$$T = \frac{1 - 2(A_0 - A_1)}{2(B_0 - B_1)}, \tag{A 11}$$

where the assumption of small polymer fraction can no longer be applied, corresponding to approximately 308 K in the ANB model and 311 K in the HHT model. This is close to the measured critical temperatures at which the affinity for water molecules drops rapidly and the gel dries out, T_C (equal to around 305 K and 307.6 K in the two cases, respectively).

Appendix B. Quantifying the coupling between lumen flow and gel dynamics

Boundary conditions on the exterior of the tube are determined based on the assumption that $p \equiv 0$ in the quiescent fluid surrounding the hydrogel tube, a reasonable assumption in an unbounded fluid bath. However, assuming that $p \equiv 0$ on the interior of the tube, where we would instead expect pressure gradients to balance viscous stresses resulting from lumen fluxes, is not a valid approach to seeking an expression for the polymer fraction at $r = b_0(z, t)$.

Making the assumption that pressures and stresses are independent of scaled radial position

$R = r/a_1$ and depend only on the distance along the tube axis, we still impose $\sigma_{rr} = 0$ at $R = B_0 = b_0/a_1$. We must solve for the Stokes flow inside the lumen that couples to the dynamics of the tube through a mixed boundary condition. Describing this flow by $\boldsymbol{v} = v_r \hat{\boldsymbol{r}} + v_z \hat{\boldsymbol{z}}$,

$$\mu_l \nabla^2 \boldsymbol{v} - \boldsymbol{\nabla} p = \boldsymbol{0} \quad \text{and} \quad \boldsymbol{\nabla} \cdot \boldsymbol{v} = 0, \tag{B 1}$$

where μ_l is the dynamic viscosity of the water in the tube. Since $p = p(Z)$, the radial component of this equation gives

$$\frac{1}{R} \frac{\partial}{\partial R} \left(R \frac{\partial v_r}{\partial R} \right) - \frac{v_r}{R^2} + \varepsilon^2 \frac{\partial^2 v_r}{\partial Z^2} = 0, \tag{B 2}$$

which, at leading order in ε, is solved by $v_r = C(Z)R$ (requiring regularity at $R = 0$). Thence, incompressibility allows us to find the form of v_z,

$$\frac{\partial v_z}{\partial Z} + \frac{1}{\varepsilon R} \frac{\partial}{\partial R} (R v_r) = 0 \quad \text{so} \quad v_z = -\frac{2}{\varepsilon} \int_0^Z C(z') \, \mathrm{d}z'. \tag{B 3}$$

This shows that, as expected, axial flows are much faster than radial flows, owing to slenderness. Substituting v_z into the axial component of equation (B 1) shows that

$$\frac{\partial p}{\partial Z} = -\frac{2\mu_l}{a_1} \frac{\partial C}{\partial Z} \quad \text{so} \quad p = -\frac{2\mu_l}{a_1} C(Z), \tag{B 4}$$

on the assumption that $p = 0$ in regions where there is no deswelling, i.e. where $C = 0$ and there is no flow. Hence, since $p + \Pi(\phi) = 0$ at the inner tube surface,

$$\phi_2 = \frac{\phi_0(T) - \phi_1}{\varepsilon^2} + \frac{2\mu_l}{\varepsilon^2 a_1 \Pi_0(T)} C(Z) \quad \text{at } R = B_0. \tag{B 5}$$

Notice that this forces both $C(Z)$ (the magnitude of the pervadic pressure corrections) and $\phi_0 - \phi_1$ to be order ε^2, corresponding to a tube where the polymer fraction is everywhere close to its equilibrium value. To find $C(Z)$, we match radial fluid velocities in the gel and the lumen,

$$v_r = \frac{D(\phi, T)}{a_1 \phi} \left. \frac{\partial \phi}{\partial R} \right|_{R=B_0} \quad \text{so} \quad C(Z) = \frac{\varepsilon^2 D(\phi_1, T)}{a_1 \phi_1 B_0} \left. \frac{\partial \phi_2}{\partial R} \right|_{R=B_0}, \tag{B 6}$$

resulting in order-ε^2 corrections to the pervadic pressure field on the inside of the tube, as expected. This combines with equation (B 5) to give a mixed boundary condition on ϕ_2 at $R = B_0$,

$$\phi_2 - \frac{2\mu_l D(\phi_1, T)}{a_1^2 \phi_1 \Pi_0(T) B_0} \left. \frac{\partial \phi_2}{\partial R} \right|_{R=B_0} = \frac{\phi_0 - \phi_1}{\varepsilon^2}. \tag{B 7}$$

To understand the relative importance of terms on the left-hand side of this boundary condition, introduce a non-dimensional coupling parameter G,

$$G \sim \frac{\mu_l D}{a_1^2 \Pi_0} \sim \frac{k}{a_1^2}, \tag{B 8}$$

scaling the diffusivity using its form in equation (3.8), $D \sim k\Pi_{00}/\mu_l$. Since we expect $k \sim 10^{-15} \, \mathrm{m}^2$ (Etzold *et al.* 2021), it is reasonable to assume $G \ll 1$ for all tubes of relaxed radius $a_1 \gtrsim 10^{-7} \, \mathrm{m}$ – hence it is possible to uncouple the interior flow from the dynamics of the inner surface of the tube, and we can assume that the same boundary condition $\phi_2 = [\phi_0(T) - \phi_1]/\varepsilon^2$ holds on the interior as on the exterior.

Appendix C. Thermoelasticity and heat transfer in gels

All hyperelastic models based on an energy density function $\mathcal{W}$ (the Helmholtz free energy) require an approach based on thermodynamics to derive the components of the stress tensor in terms of the deformation (Zaoui & Stolz 2001). A number of recent works have sought models that couple chemical diffusion, thermodynamics and swelling to model thermo-responsive gels, but these are usually formulated in terms of energy density functions and not the Eulerian continuum-mechanical quantities in this study (Brunner *et al.* 2024). Following a standard approach pioneered by Coleman & Noll (1963), and detailed in Chester & Anand (2011) and Drozdov (2014), we can write down an expression for the internal energy of a hydrogel per unit volume,

$$\frac{\mathrm{d}U_d}{\mathrm{d}t} = R_d - \boldsymbol{\nabla_d} \cdot \boldsymbol{Q_d} + \boldsymbol{P} : \frac{\mathrm{d}\boldsymbol{F_d}}{\mathrm{d}t} + \mu \frac{\mathrm{d}C_d}{\mathrm{d}t} - \boldsymbol{J_d} \cdot \boldsymbol{\nabla_d}\mu, \tag{C 1}$$

where R_d is the external supply of heat per unit volume, C_d is the number density of water molecules per unit reference volume, μ is the chemical potential, $\boldsymbol{Q_d}$ is the heat flux, T is the temperature, $\boldsymbol{J_d}$ is the flux of water molecules, $\boldsymbol{F_d}$ is the deformation gradient tensor from a dry reference state and $\boldsymbol{P}$ is the first Piola-Kirchhoff stress tensor. The subscript $_d$ references quantities measured relative to a 'dry' reference state where $\phi \equiv 1$ (as detailed, for example, in equation (A 2)).

In an Eulerian reference frame, it is standard to take Fourier's law of conduction to describe the heat flux $\boldsymbol{Q}$, and the molecular flux of water $\boldsymbol{J}$ is simply found by dividing the relative fluid volume flux by the volume of a single water molecule Ω_f, such that

$$\boldsymbol{Q} = -\rho c \kappa \boldsymbol{\nabla} T \quad \text{and} \quad \boldsymbol{J} = -\frac{k(\phi)}{\mu_l \Omega_f} \boldsymbol{\nabla} p, \tag{C 2}$$

where ρ is the material density, c is the specific heat capacity and κ is the thermal diffusivity. Furthermore, an expression for C_d can be found by appealing to incompressibility of water and polymer phases, such that any increases in volume from the dry state are due to the addition of water molecules alone, and hence

$$C_d = \frac{\phi^{-1} - 1}{\Omega_f} \quad \text{so} \quad \frac{\mathrm{d}C_d}{\mathrm{d}t} = -\frac{1}{\Omega_f \phi^2} \frac{\mathrm{d}\phi}{\mathrm{d}t}. \tag{C 3}$$

In order to rewrite the energy balance of equation (C 1) in an Eulerian form instead of its usual Lagrangian form with reference to a dry state, we make use of the assumption of LENS modelling that all deformation is, at leading order, isotropic. Hence,

$$\boldsymbol{F} \approx \left(\frac{\phi}{\phi_0}\right)^{-1/3} \boldsymbol{I} \quad \text{so} \quad \boldsymbol{F_d} \approx \phi^{-1/3} \boldsymbol{I}, \tag{C 4}$$

making use of the relation between $\boldsymbol{F}$ and $\boldsymbol{F_d}$ presented in equation (A 2). This governing assumption also allows us to replace all instances of $\boldsymbol{\nabla_d}$ with $\phi^{-1/3}\boldsymbol{\nabla}$ at leading order in the deviatoric strain, since the Eulerian state is approximately an isotropic dilatation of the fully-dry polymer reference state. The Piola-Kirchhoff and Cauchy strains are related via

$$\boldsymbol{P} = \phi^{-1}\sigma\boldsymbol{F_d}^{-T} \approx \phi^{-2/3}\sigma \quad \text{hence} \quad \boldsymbol{P} : \frac{\mathrm{d}\boldsymbol{F_d}}{\mathrm{d}t} \approx -\frac{1}{3\phi^2} \frac{\mathrm{d}\phi}{\mathrm{d}t} \operatorname{tr}\sigma. \tag{C 5}$$

Finally, since lengths scale with $\phi^{-1/3}$ from the dry state to the swollen state, and volumes correspondingly by ϕ^{-1},

$$U = \phi U_d, \quad R = \phi R_d, \quad \boldsymbol{Q} = \phi^{2/3}\boldsymbol{Q_d} \quad \text{and} \quad \boldsymbol{J} = \phi^{2/3}\boldsymbol{J_d}, \tag{C 6}$$

and hence equation (C 1) can be rewritten as

$$\frac{\mathrm{d}}{\mathrm{d}t}\left(\frac{U}{\phi}\right) = \frac{R}{\phi} - \phi^{-1/3}\boldsymbol{\nabla}\cdot\left(\phi^{-2/3}\boldsymbol{Q}\right) - \frac{\mu}{\Omega_f\phi^2}\frac{\mathrm{d}\phi}{\mathrm{d}t} - \frac{1}{\phi}\boldsymbol{J}\cdot\boldsymbol{\nabla}\mu - \frac{1}{3\phi^2}\frac{\mathrm{d}\phi}{\mathrm{d}t}\operatorname{tr}\sigma$$

$$= \frac{R}{\phi} + c\kappa\phi^{-1/3}\boldsymbol{\nabla}\cdot\left(\phi^{-2/3}\boldsymbol{\nabla}T\right) - \frac{\mu}{\Omega_f\phi^2}\frac{\mathrm{d}\phi}{\mathrm{d}t} + \frac{k(\phi)}{\mu_l\Omega_f\phi}\boldsymbol{\nabla}p\cdot\boldsymbol{\nabla}\mu - \frac{1}{3\phi^2}\frac{\mathrm{d}\phi}{\mathrm{d}t}\operatorname{tr}\sigma.$$
$$(\text{C}\,7)$$

Expanding all terms of this equation and noting that the pervadic pressure and chemical potential are related by $p = \mu/\Omega_f$ alongside $\operatorname{tr}\sigma = -3(p + \Pi)$,

$$\frac{\mathrm{d}}{\mathrm{d}t}\left(\frac{U}{\phi}\right) = \frac{R}{\phi} + \frac{\rho c\kappa}{\phi}\nabla^2 T - \frac{2\rho c\kappa}{3\phi^2}\boldsymbol{\nabla}\phi\cdot\boldsymbol{\nabla}T + \frac{k(\phi)}{\mu_l\phi}|\boldsymbol{\nabla}p|^2 + \frac{\Pi(\phi)}{\phi^2}\frac{\mathrm{d}\phi}{\mathrm{d}t}. \qquad (\text{C}\,8)$$

Now, if the internal energy is given by ρcT and the added assumption that density remains approximately constant in time is made,

$$\frac{\mathrm{d}T}{\mathrm{d}t} = \frac{R}{\rho c} + \kappa\nabla^2 T - \frac{2\kappa}{3\phi}\boldsymbol{\nabla}\phi\cdot\boldsymbol{\nabla}T + \frac{k(\phi)}{\rho c\mu_l}|\boldsymbol{\nabla}p|^2 + \frac{1}{\phi}\left(\frac{\Pi(\phi)}{\rho c} + T\right)\frac{\mathrm{d}\phi}{\mathrm{d}t}. \qquad (\text{C}\,9)$$

LENS scalings show that gradients in polymer fraction are small on the order of the deviatoric strain, and therefore the $\boldsymbol{\nabla}\phi\cdot\boldsymbol{\nabla}T$ term is much smaller than that featuring $\nabla^2 T$. Furthermore, we can replace the total derivatives with the material derivative advecting with the polymer scaffold, so the leading order temperature evolution equation is

$$\frac{\partial T}{\partial t} + \boldsymbol{q}\cdot\boldsymbol{\nabla}T = \frac{R}{\rho c} + \kappa\nabla^2 T + \frac{k(\phi)}{\rho c\mu_l}|\boldsymbol{\nabla}p|^2 + \frac{1}{\phi}\left(\frac{\Pi(\phi)}{\rho c} + T\right)\left(\frac{\partial\phi}{\partial t} + \boldsymbol{q}\cdot\boldsymbol{\nabla}\phi\right). \qquad (\text{C}\,10)$$

This heat equation shows how temperature evolves due to material fluxes (the advective term), diffusion, and then two additional terms related to swelling and internal flows. The first term is equal to $(\boldsymbol{u}\cdot\boldsymbol{F})/\rho c$ where $\boldsymbol{F} = -\boldsymbol{\nabla}p$ and so represents the rate of work done by the pervadic pressure gradients in the interstitial flow. The second, related to the osmotic pressure and changes in polymer fraction, arises as energy is either used up or released as water molecules associate and dissociate with polymer chains, and can hence be seen as an analogue of latent heat in phase change.

REFERENCES

ABRAMOWITZ, M. & STEGUN, I. A. 1970 *Handbook of Mathematical Functions: with Formulas, Graphs, and Mathematical Tables*. National Bureau of Standards.

AFROZE, F., NIES, E. & BERGHMANS, H. 2000 Phase transitions in the system poly(N-isopropylacrylamide)/water and swelling behaviour of the corresponding networks. *J. Mol. Struct.* **554** (1), 55–68.

BERTRAND, T., PEIXINHO, J., MUKHOPADHYAY, S. & MACMINN, C. W. 2016 Dynamics of swelling and drying in a spherical gel. *Phys. Rev. Appl.* **6** (6), 064010.

BRUNNER, F., SEIDLHOFER, T. & ULZ, M. H. 2024 A numerical model for chemo-thermo-mechanical coupling at large strains with an application to thermoresponsive hydrogels. *Comput. Mech.* **74**, 509–536.

BUTLER, M. D. & MONTENEGRO-JOHNSON, T. D. 2022 The swelling and shrinking of spherical thermo-responsive hydrogels. *J. Fluid Mech.* **947**, A11.

CAI, S. & SUO, Z. 2011 Mechanics and chemical thermodynamics of phase transition in temperature-sensitive hydrogels. *J. Mech. Phys. Solids* **59** (11), 2259–2278.

CAI, S. & SUO, Z. 2012 Equations of state for ideal elastomeric gels. *EPL* **97** (3), 34009.

CHESTER, S. A. & ANAND, L. 2011 A thermo-mechanically coupled theory for fluid permeation in elastomeric materials: Application to thermally responsive gels. *J. Mech. Phys. Solids* **59**, 1978–2006.

COLEMAN, B. D. & NOLL, W. 1963 The thermodynamics of elastic materials with heat conduction and viscosity. *Arch. Ration. Mech. Anal.* **13** (1), 167–178.

CURATOLO, M., LISI, F., NAPOLI, G. & NARDINOCCHI, P. 2023 Circumferential buckling of a hydrogel tube emptying upon dehydration. *Eur. Phys. J. Plus* **138**, 382.

CURATOLO, M., NARDINOCCHI, P. & TERESI, L. 2018 Driving water cavitation in a hydrogel cavity. *Soft Matt.* **14**, 2310–2321.

DAS, D., GHOSH, P., GHOSH, A., HALDAR, C., DHARA, S., PANDA, A. B. & PAL, S. 2015 Stimulus-responsive, biodegradable, biocompatible, covalently cross-linked hydrogel based on dextrin and poly(N-isopropylacrylamide) for in vitro/in vivo controlled drug release. *ACS Appl. Mater. Interfaces* **7**, 14338–14351.

DOI, M. 2009 Gel dynamics. *J. Phys. Soc. Jpn.* **78** (5), 052001.

DONG, L. & JIANG, H. 2007 Autonomous microfluidics with stimuli-responsive hydrogels. *Soft Matter* **3**, 1223–1230.

DROZDOV, A. D. 2014 Swelling of thermo-responsive hydrogels. *EPJE* **37** (10), 93.

ETZOLD, M. A., LINDEN, P. F. & WORSTER, M. G. 2021 Transpiration through hydrogels. *J. Fluid Mech.* **925**, A8.

FENG, Y., GERBER, D., HEYDEN, S., KRÖGER, M., DUFRESNE, E. R., ISA, L. & STYLE, R. 2024 Characterizing hydrogel behavior under compression with gel-freezing osmometry. *arXiv preprint 2407.13718* .

FREEMAN, J. J., MORGAN, G. J. & CULLEN, C. A. 1987 Thermal conductivity of a single polymer chain. *Phys. Rev. B* **35**, 7627–7635.

GOMEZ, M., MOULTON, D. & VELLA, D. 2017 Critical slowing down in purely elastic 'snap-through' instabilities. *Nature Phys.* **13**, 142–145.

GUILHERME, M. R., AOUADA, F. A., FAJARDO, A. R., MARTINS, A. F., PAULINO, A. T., DAVI, M. F. T., RUBIRA, A. F. & MUNIZ, E. C. 2015 Superabsorbent hydrogels based on polysaccharides for application in agriculture as soil conditioner and nutrient carrier: A review. *Eur. Polym. J.* **72**, 365–385.

HARMON, M. E., TANG, M. & FRANK, C. W. 2003 A microfluidic actuator based on thermoresponsive hydrogels. *Polymer* **44** (16), 4547–4556.

HENNESSY, M. G., MÜNCH, A. & WAGNER, B. 2020 Phase separation in swelling and deswelling hydrogels with a free boundary. *Phys. Rev. E* **101** (3), 032501.

HIROTSU, S., HIROKAWA, Y. & TANAKA, T. 1987 Volume-phase transitions of ionized N-isopropylacrylamide gels. *J. Chem. Phys.* **87** (2), 1392–1395.

KAVIANY, M. 1995 *Principles of Heat Transfer in Porous Media*. Springer New York.

LEE, Y., SONG, W. J. & SUN, J. Y. 2020 Hydrogel soft robotics. *Mater. Today Phys.* **15**, 100258.

LI, J., HU, Y., VLASSAK, J. J. & SUO, Z. 2012 Experimental determination of equations of state for ideal elastomeric gels. *Soft Matt.* **8** (31), 8121–8128.

MASLEN, C., GHOLAMIPOUR-SHIRAZI, A., BUTLER, M. D., KROPACEK, J., REHOR, I. & MONTENEGRO-JOHNSON, T. D. 2023 A new class of single-material, non-reciprocal microactuators. *Macromol. Rapid Commun.* **44** (6), 2200842.

MATSUO, E. S. & TANAKA, T. 1988 Kinetics of discontinuous volume–phase transition of gels. *J. Chem. Phys.* **89**, 1695–1703.

NEUMANN, M., DI MARCO, G., IUDIN, D., VIOLA, M., VAN NOSTRUM, C. F., VAN RAVENSTEIJN, B. G. P. & VERMONDEN, T. 2023 Stimuli-responsive hydrogels: the dynamic smart biomaterials of tomorrow. *Macromolecules* **56** (21), 8377–8392.

NISTANE, J., CHEN, L., LEE, Y., LIVELY, R. & RAMPRASAD, R. 2022 Estimation of the Flory-Huggins interaction parameter of polymer-solvent mixtures using machine learning. *MRS Commun.* **12**, 1096–1102.

PEPPIN, S. S. L., ELLIOTT, J. A. W. & WORSTER, M. G. 2005 Pressure and relative motion in colloidal suspensions. *Phys. Fluids* **17** (5), 053301.

PETERSEN, K. B. & PEDERSEN, M. S. 2012 The Matrix Cookbook, November 2012. *Technical University of Denmark* **7** (15).

REDDY, J. N. 2013 *An Introduction to Continuum Mechanics, Second Edition*. Cambridge University Press.

RICHTER, A., KLATT, S., PASCHEW, G. & KLENKE, C. 2009 Micropumps operated by swelling and shrinking of temperature-sensitive hydrogels. *Lab Chip* **9**, 613–618.

SALENÇON, J. 2007 *Mécanique des milieux continus - II, Thermoélasticité*. Éditions de l'École Polytechnique.

SEO, J., WANG, C., CHANG, S., PARK, J. & KIM, W. 2019 A hydrogel-driven microfluidic suction pump with a high flow rate. *Lab Chip* **19**, 1790–1796.

SPRATTE, T., ARNDT, C., WACKER, I., HAUCK, M., ADELUNG, R., SCHRÖDER, R. R., SCHÜTT, F. & SELHUBER-

30

UNKEL, C. 2022 Thermoresponsive hydrogels with improved actuation function by interconnected microchannels. *Adv. Intell. Sys.* **4**, 2100081.

TOMARI, T. & DOI, M. 1995 Hysteresis and incubation in the dynamics of volume transition of spherical gels. *Macromolecules* **28**, 8334–8343.

VERNEREY, F. & SHEN, T. 2017 The mechanics of hydrogel crawlers in confined environment. *J. R. Soc. Interface* **14** (132), 20170242.

VOUDOURIS, P., FLOREA, D., VAN DER SCHOOT, P. & WYSS, H. M. 2013 Micromechanics of temperature sensitive microgels: dip in the Poisson ratio near the LCST. *Soft Matter* **9**, 7158–7166.

WEBBER, J. J. 2024 Dynamics of super-absorbent hydrogels. PhD thesis, University of Cambridge.

WEBBER, J. J., ETZOLD, M. A. & WORSTER, M. G. 2023 A linear-elastic-nonlinear-swelling theory for hydrogels. Part 2. Displacement formulation. *J. Fluid Mech.* **960**, A38.

WEBBER, J. J. & WORSTER, M. G. 2023 A linear-elastic-nonlinear-swelling theory for hydrogels. Part 1. Modelling of super-absorbent gels. *J. Fluid Mech.* **960**, A37.

XU, S., CAI, S. & LIU, Z. 2018 Thermal conductivity of polyacrylamide hydrogels at the nanoscale. *ACS Appl. Mater. Interfaces* **10**, 36352–36360.

XU, Z., YUE, P. & FENG, J. J. 2024 A theory of hydrogel mechanics that couples swelling and external flow. *Soft Matt.* **20**, 5389–5406.

XU, Z., ZHANG, J., YOUNG, Y.-N., YUE, P. & FENG, J. J. 2022 Comparison of four boundary conditions for the fluid–hydrogel interface. *Phys. Rev. Fluids* **7**, 093301.

ZAOUI, A. & STOLZ, C. 2001 Elasticity: Thermodynamic Treatment. *Encyclopedia of Materials: Science and Technology* pp. 2445–2448.

ZOHURIAAN-MEHR, M. J., OMIDIAN, H., DOROUDIANI, S. & KABIRI, K. 2010 Advances in non-hygienic applications of superabsorbent hydrogel materials. *J. Mater. Sci.* **45** (21), 5711–5735.